Ph. D. Dissertation of Engineering

Photo actuation of azobenzene incorporated liquid crystalline elastomers : fabrication and analysis study

광반응 탄성체기반 액츄에이터의 거동 메커니즘 연구

August 2022

Graduate School of Mechanical Engineering

Seoul National University

Hyunsu Kim

Photo actuation of azobenzene incorporated liquid crystalline elastomers : fabrication and analysis study

Academic advisor: 안 성 훈

Submitting a Ph.D. Dissertation of Engineering

April 2022

Graduate School of Mechanical Engineering

Seoul National University

Hyunsu Kim

Confirming the Ph.D. Dissertation written by

Hyunsu Kim

June 2022

Chair	고 승 환	**(Seal)**
Vice Chair	안 성 훈	**(Seal)**
Examiner	이 윤 석	**(Seal)**
Examiner	윤 정 훈	**(Seal)**
Examiner	이 규 희	**(Seal)**

Abstract

Hyunsu Kim

Department of Mechanical Engineering

The Graduate School

Seoul National University

Azobenzene incorporated liquid crystalline elastomers (azo-LCEs) is contains azobenzene in there molecule network, and it occur photo-isomerization when PRP-LCEs irradiated UV-light. Azo-LCEs can potentially be used in diverse applications, such as soft robot, sensors, and actuators, because of their reversibility, remote-controllability, and immediateness of the response. However, real world applications of azo-LCEs are lacking because of the strains generated by irradiation of light are not so large, and the work capacity is not suitable to apply.

Here, we report an azo-LCEs constructed with thiol-click Michael addition reaction. Azo LCEs shows dual stimuli shape memory cycle triggered by force/heat and light. In particular during photo deformation process, azo LCEs shows not only huge actuation (up to 26%) under the stress condition but also shows the higher work capacity than mammalian muscle (up to 77J/Kg). To better understand, we control the molecule structure system by using change of crosslinker concentration and sequential polymerization process. When azobenzene in the molecules network occur photo-isomerization, not only the isomerization effect of the azobenzene itself but also influence of tuned nematic-isotropic transition temperature of azo-LCEs molecule network contribute to make immediately huge actuation. Since the photo-isomerization of azobenzene and the external loading force applied to azo-LCEs have a complex effect on this transition temperature shifting, we constructed an in-situ experimental system to better understand this phenomenon. Our azo-LCE has not only shown that it has conditions that can be used in various applications including artificial muscles, but is also expected to be used importantly in various fields for future actuators and their mechanism studies.

Keyword: Liquid crystalline elastomers, Azobenzene incorporated elastomers actuator, artificial muscle based on LCEs

Student Number: 2018-30325

Table of Contents

Chapter 1. Introduction

1.1 Multi-functional polymer-based smart actuator

As the material paradigm begins to be widely applied to biomimicry technology and biotechnology, it is flexible and sometimes the material itself to solve problems such as the limitation of functionality and the limitation of the scope of application due to the material characteristics of the existing rigid material. Research on flexible-intelligent materials with intelligence is being actively conducted.[1,2] These materials are composed of polymers and composite polymers, and due to the characteristics of polymers, they show higher sensitivity to external environments such as temperature and pressure than conventional rigid materials, and require an organic linkage methodology between structural design and material design.[3]

Recently, as the importance of soft application has emerged, researches on flexible and large deformation materials unlike the existing materials are being actively conducted. These materials are called ‘smart materials’ cause these can actuate by stimulate such as thermal, electron, PH, humidity, and light.[4,5] Unlikely conventional actuator and applications, soft robots and actuator often do not have an actuation part, but the whole actuator is a working part, and the material itself makes smart deformation. So that, smart materials need huge actuation range, flexibility, and fast responsibility.

Up to date, the possibility and potential to function as a smart actuator has been explored in numerous polymer material systems, such as polymeric (hydro-) gel, cross-linked elastomers, liquid crystalline polymers and molecular crystals.[6-8] Moreover, various actuation mechanisms were developed to achieve the fundamental goal: the volumetric changes. Based on different stimulations and working condition requirements, the actuation mechanisms varies from (photo-) thermal-expansion (contraction), electric static force, microscale phase changes to small molecule/ionic diffusions.[9-11]

1.2 Liquid crystalline polymer

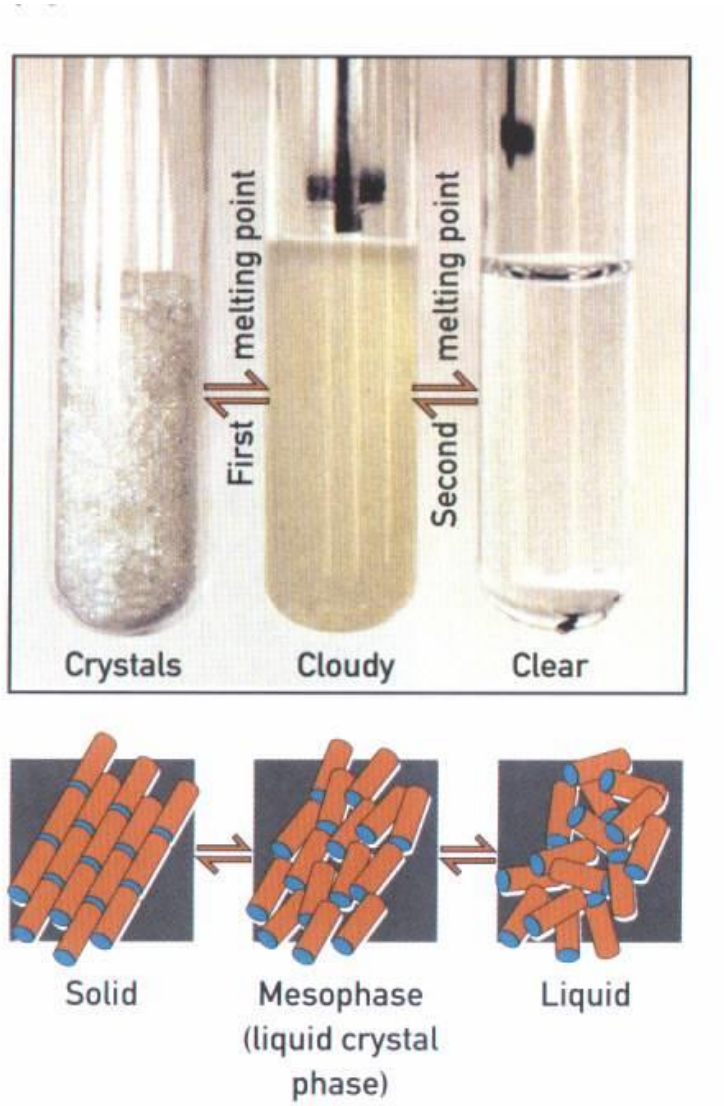

Figure 1. Phase transition of liquid crystal molecular in test tubes. The liquid crystal phase appears to be cloudy with molecules can move about but still pointing towards the same directions.[12]

Liquid crystals are synthetic organic molecules that will change, upon heating up, their original crystalline solid phase into a fourth phase, where the system could preserve the anisotropic characteristics, yet could flow like liquids. Because of their ability of self-assembling into aligned states such as including nematic, smectic, chiral, blue, discotic or bowlic phases, liquid crystal molecules are widely used in digital displays, optical components and *et al*.[13]

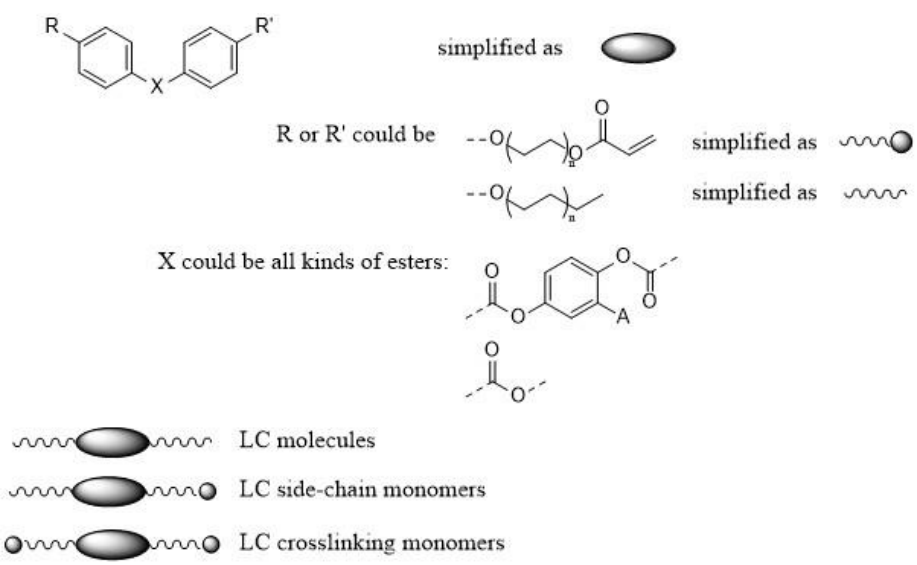

Figure 2. The building blocks of LC monomers used in this thesis and their simplified molecule schemes.

Liquid crystals molecules with functional groups that are capable of being polymerized (such as acrylic, vinylether, epoxide or oxetane), are usually referred as "liquid crystal monomers". **Figure 2** demonstrates the basic building block of the acrylic liquid crystal monomers, and schemes of two different monomers: crosslinkers and side chain monomers used in this thesis. Once polymerized in their mesophases, liquid crystal monomers will self-form anisotropic polymer structures that are capable of reversely undergo volumetric changes when phase transition (e.g. nematic to isotropic) takes place upon the stimulation.

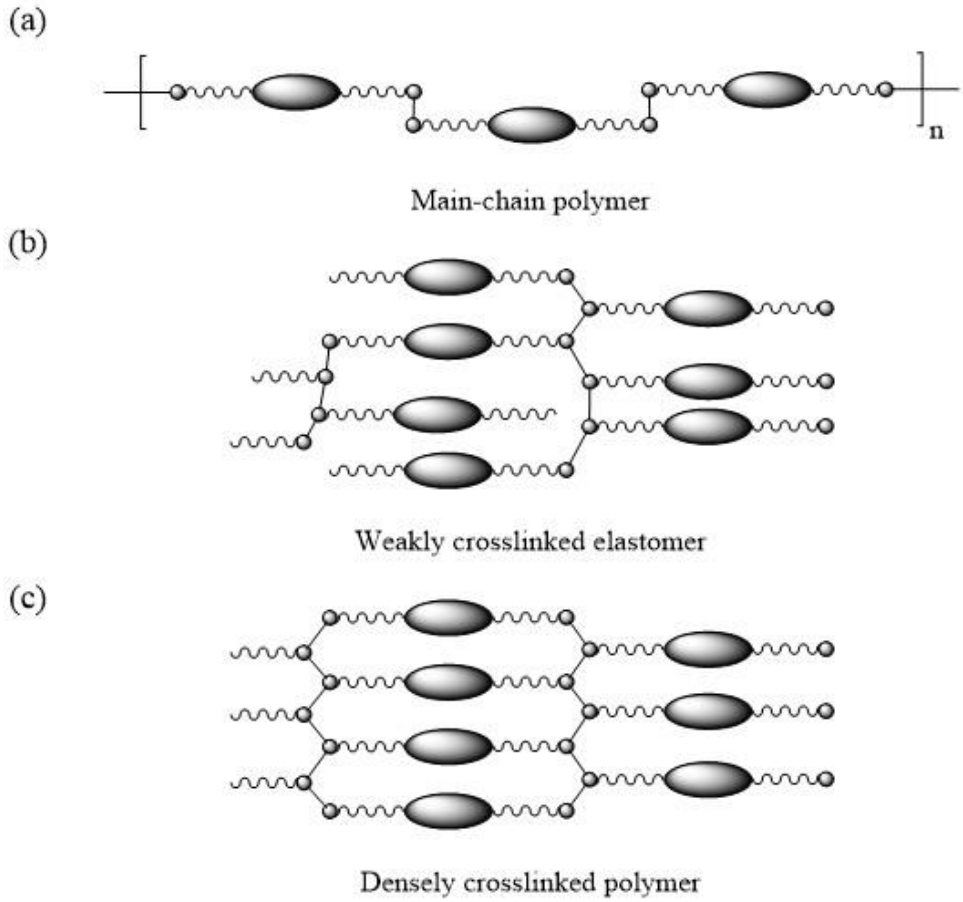

Figure 3. Schemes of different types of LC polymeric structures. (a) main-chain LC polymer (b) weakly cross-linked elastomer and (c) densely cross-linked polymer.

Depends on the method of polymerization as well as the number of polymer functionalized groups in the system, several types of LCPs could be achieved. **Figure3** shows three typical structures of liquid crystalline polymer networks: main-chain, weakly cross-linked and densely cross-linked polymers. While main-chain and weakly cross-linked elastomers are widely used as thermoplastics and one-way SMPs **Figure4** a) and b), this thesis will focus on the densely cross-linked liquid crystalline polymers..[14]

Densely cross-linked liquid crystalline polymers are one of the extreme cases in polymeric structures. Because all of the monomers used in the polymer are cross-linkers, the polymer shows extremely high crosslinking densities (> 40 mol/dm^3). The ultra-high crosslinking density offers outstanding thermo-mechanical properties (high strength, modulus and T_g) and also long-term stability, chemical resistivity and reliable actuation life when heated above the T_g. However, because of the low mesogen mobility and high π - π staking energy, the densely cross-linked polymer usually have high activation temperature for actuation (usually > 80 °C). [15]

This chapter cites Ph.D Li Chenzhe's 2018 Ph.D dissertation's 'Chapter 1.3 : Liquid crystalline glassy actuators'.

1.3 Azobenzene incorporated liquid crystalline elastomers

Polymer actuators with high power output and working capacity are important for many applications, such as microelectronics, microfluidic chips and soft robotics. [1, 16-18] Photo-responsive polymer actuators are of great interest because light carries controlling signals and high energy density power supply spontaneously with up to sub-micro scale spatial selectivity.[19-23] Such type of actuators could potentially be applied to light-controlled soft robots, shape morphing devices and optical switches. [24-26] One of the effective strategies for the implementation of photo-responses in polymer actuators is to exploit the photo-isomer (such as azobenzene, diarylethene and spiropyran) produced microscopic reversible molecular motions under light irradiation.[27-31] The photoisomerization of azobenzene and its derivatives generates microscale shrinkage along the molecular long-axis by changing the molecular structure from rod-shaped *trans*-state to v-shaped *cis*-state.[32] This process can be activated by short wavelength light (usually UV or blue) irradiation and recovered by the illumination of visible light (usually > 450 nm). [33]

Liquid crystalline elastomers (LCEs) exhibit various phases depending on the flexibility of the material itself and the environment, and many studies have been conducted because it can be applied to a wide range.[34] Especially azobenzene incorporated liquid crystalline elastomers make huge deformation under the light irradiation.[35-37] As such, photo responsive LCEs has been actively studied experimentally and dynamically by research groups such as T.J White, Ikeda and coworkers.[38-40] Due to these characteristics, studies on the reaction repeatability, actuation, and mechanical properties of azobenzene incorporated elastomers in which azobenzene monomers substituted with reaction groups are grafted onto the elastomer systems such as polydimethylsiloxane (PDMS) system, thiol based system, and epoxy system have been actively studied. [41-42]

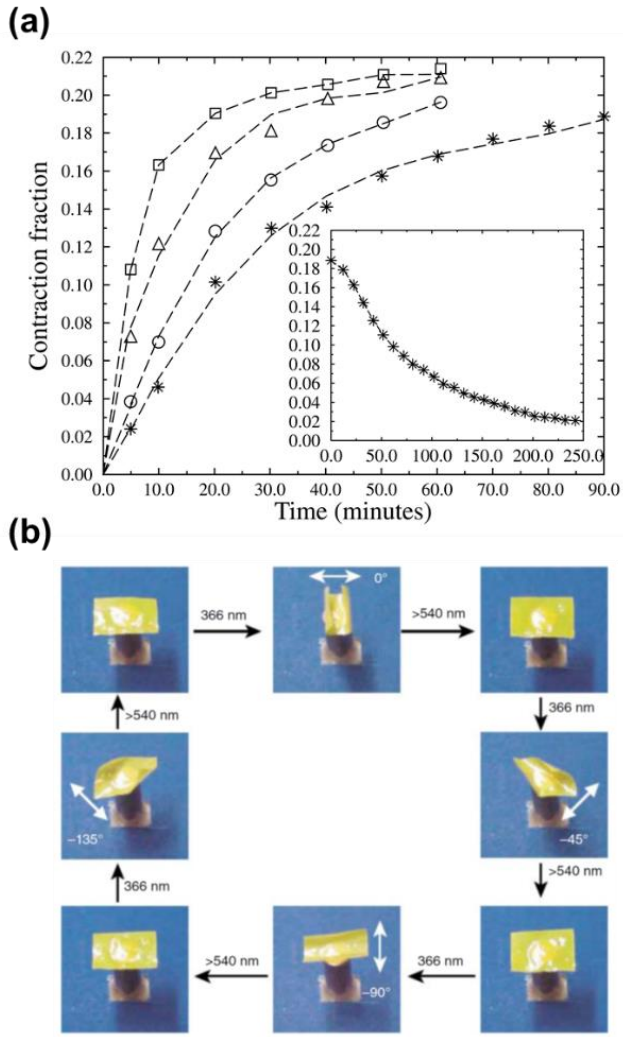

Figure 4. (a) Photo induced contraction as a function of time for an azobenzene incorporated liquid crystal elastomer upon UV irradiation. (Figure reproduced from Ref. [43]) (b) All optical control of bending direction and flattening in an azo-LCP . (Figure reproduced from Ref [44].)

Among them, we studied azobenzene incorporated elastomers (azo-LCEs) system consisting of polymerization between crosslinkers with thiol reaction group and liquid crystalline monomer and azobenzene monomer with acrylate reaction group. These azo-LCEs are characterized by the fact that they not only behave in a specific wavelength region (ultra violet region and visible light region) of light according to the alignment direction but also cause phase transition.

The phase transition is one of the most important properties of a liquid crystalline polymer because the mechanical, thermal, and optical properties completely change depending on the phase of liquid crystalline polymer, and the application range of the polymer is completely changed accordingly. In conventional liquid crystalline elastomers (LCEs), a phase transition occurs due to temperature change and external force, but azobenzene incorporated PRP-LCEs also undergo a phase transition due to photo-isomerization of azobenezene in the molecule network. When UV light are irradiated to the PRP-LCEs, photo-isomerization of azobenzene inside the molecule network from the trans state to the cis state occurs, which not only changes the shape of azobenzene, but also changes the entire molecule network. In this process, the arrangement of the liquid crystal mesogen of the PRP-LCEs molecule network is disturbed and changes to the isotropic phase.

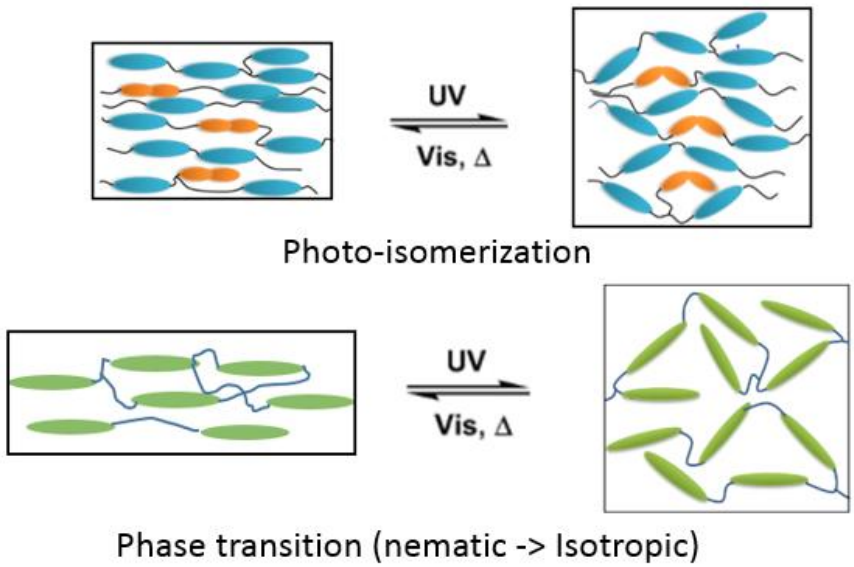

Figure 5. Scheme of photo-isomerization and phase transition due to the photo-isomerization. [45]

However, when an external force of more than a certain strength is acting, even if isomerization occurs in LCEs, the isotropic state cannot be established and the nematic phase maintained depending on the strength of the applied force. As described above, the effects of conditions such as temperature and external force also have a complex effect. For these reasons, the phase transition of PRP-LCEs becomes a very complex problem. Studies on the deformation or photo-softening effect due to photo-isomerization of azobenzene in the azobenzne incorporated polymer network have been steadily progressed.

Our research team has conducted research on the effect of external loads on the photo softening effect of azobenzene incorporated liquid crystalline polymer. We confirmed the large deformation and shape memory effect that this material makes by light, and analyzed/researched the deformation in terms of the change of transition temperature due to azobenzene isomerization. When an UV-irradiation is applied under the external force condition, a property change occurs due to photo-isomerization of azobenzene incorporated polymer. The influence of the intensity of external loading force on property change was studied.

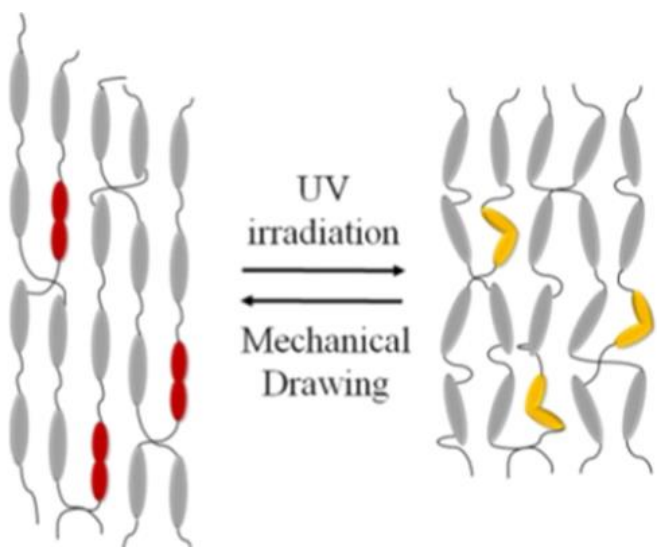

Figure 6. Scheme of molecule network structure change due to the photo-isomerization. [46]

1.4 Polymer alignment under the preloading force

The photomechanical behavior of azobenzene incorporated liquid crystalline polymers (azo-LCP) is closely related to the applied external loadings.[5] The effect of loadings on the photo-induced strain by comparing two different LC hosts systems is reported from our research group.[47,48] Dynamic mechanical analysis revealed that photo-induced strain decreases following two-phase character as loading increases. In-situ spectrometer studies and molecular dynamic simulation show that both LC mesogen rotation as well as azobenzene isomerization resulted big modulus change are responsible for rapid strain decrease under relatively low loadings; while only azobenzene isomerization contributes to the linear gentle strain-loading relationship under high loading circumstances. As the result, in samples with higher modulus, maximum power output densities are found 3 times higher than those with lower modulus. On the other hand, we have also found that the threshold loadings (loadings azo-LCP fail to actuate) is independent from the irradiation intensities.

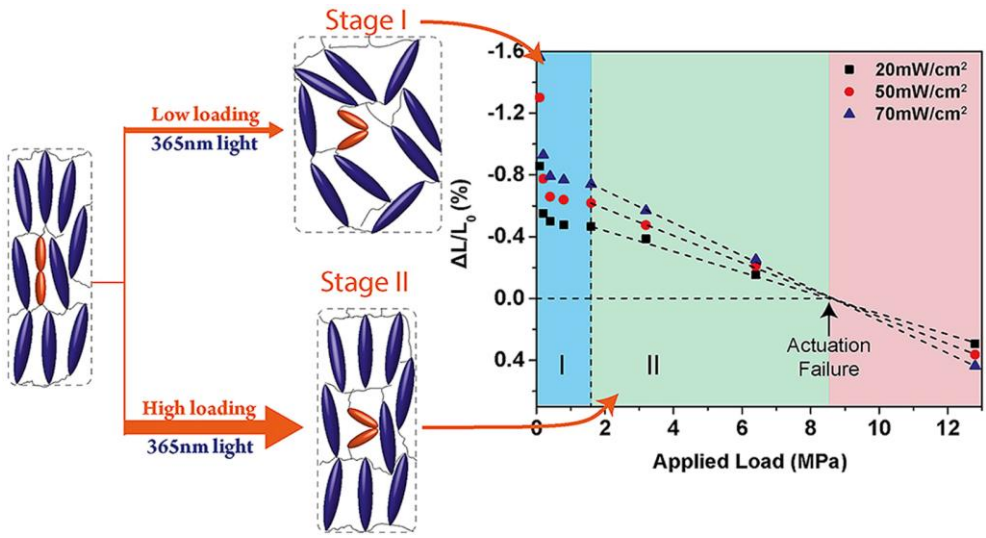

Figure 7. Photo induced contraction as a function of time for an azobenzene incorporated liquid crystal elastomer upon UV irradiation. [47]

For Azo-LCP to be used in practice, it is important to understand the property of the photomechanical response under external loading. Previous studies have suggested that the actuation strain of an isotropic polymer actuator followed a linear relationship with the external load applied to the actuator. Modulus before and after actuation was also found to play an important role in the slope of the linear relationship. The self-assembled anisotropic polymer network of azo-LCP and the photo-chemically reactive azobenzene moieties simultaneously interact with each other to generate a complex system that differs from previously reported systems. We have shown how an external load alters the optical operation in azo-LCPs. By combining the experiments with computer simulations, we found that light-induced strain was not only strongly related to the modulus change during operation, but also highly dependent on the polymer network structure under load. We demonstrated these observations using two different LC hosts with the same molecular arrangement but different modulus.

1.5 Sequential polymerization

The properties of the polymer are not only determined by the monomer chemical structures and physical architectures, but also the monomer sequences and distributions. With artificially controlled monomer distributions, sequence-controlled polymers can have very different properties comparing to the random polymers with the same composites.[49,50] Several recently studies have also demonstrated promising mechanical property and actuation response enhancement in interpenetrated polymer networks.[51-53] In the past few decades, many technologies (such as atom transfer radical polymerization (ATRP), reversible addition−fragmentation polymerization (RAFT) and templated polymerization) have been developed to manipulate the monomer distributions in the polymer. [54,55] Among the technologies, the thiol-ene sequential polymerization method provides an efficient and adaptive way to constructing sequence-controlled polymers. [56-58]

Conventionally, this method involves two step hydrothiolation reactions between multifunctional thiol monomers and different types of unsaturated hydrocarbons. In first step procedure, a chemoselective thiol-Michael addition reacted is carried to form oligomers or preliminary polymer networks. Because this reaction can only proceed within "activated" alkenes (e.g. acrylate, maleimide derivatives and fumarate esters), it offers good chemoselectivity over the other alkenes.[59,60] The second step of the polymerization takes advantage of the free-radical mediated thiol-ene "click reactions", which can be easily initiated under different conditions (e.g. photo, or thermal initiation) and often provides rapid and quantitative conversions.[61]

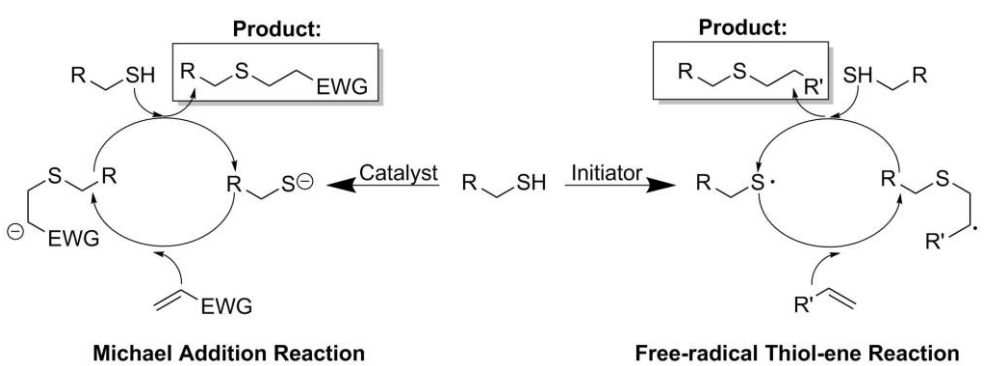

Figure 8. Mechanism for the orthogonal thiol-ene "Click" reactions used in this work.

By utilizing the scheme of two-step orthogonal thiol-ene "click" reactions, herein, we report a facile one-pot method for the preparation of azobenzene-interconnected photo-responsive polymers (azo-ICPRPs). The synthesized azo-ICPRPs can take advantage of both deep UV penetration profile and fast responses of the interconnected isomers owning to the two-step polymerization process and UV transparent substrate. While multiple types of thiol-ene reaction exists, we specifically use the thiol-acrylate and thiol-allyl as the reaction pair (**Figure 8**). By selecting the ideal nucleophile catalyst, azobenzene prepolymers (azo-prepolymer) can readily be prepared *in situ* in the first step thiol-Michael reaction. The AB-type azobenzene chain stopper is used for the molecular weight control of the azo-prepolymers. The resulted molten reaction mixtures can be injection molded before the second step polymerization. In the second step, the formed azo-prepolymers are further copolymerized with the di-allyl and tetrathiol monomers by free-radical initiated thiol-ene "Click" reaction, yielding a crosslinked co-polymer system. The as-synthesized actuators are found not only providing reversible high photo-strain actuations under external forces, but also with enhanced the mechanical properties. More importantly, we have found higher interconnected isomers (higher azo-prepolymer M_n) lead to much higher specific work and power outputs under external applied forces, which offers new aspect for the future development of isomer

incorporated actuators.

1.6 Scope and aim

The smart materials which have multi functionality or reactivity with external stimuli has been actively studied these days. Especially, azobenzene incorporated polymer which respond to ultra-violet region (360nm) and visible light region (nearby 430nm) of wavelength with light is one of the most promising materials can be hospitalized to soft application. However, the deformation amount and work capacity are still not enough to applied, and understanding of the actuation mechanism is also insufficient. The aim of this thesis is to introduce a novel properties such as huge deformation triggered by light irradiation and considerable work capacity at that actuation of film shape azo-LCEs. And also conduct on the properties and mechanism of the azo-LCEs on molecular network system and stimuli came from irradiation and preloading force. Not only immediately and huge photo-actuation which has work capacity overwhelming the mammalian muscle's work capacity but also the photo actuation mechanism were analyzed on the various factors such as crosslinking density effect, loading force effect, and polymerization effect. Consequently, the crucial information and understanding of the azo-LCEs were reported to apply to various field such as soft robotics, sensor, and actuator as a promising materials.

1.7 Outline of dissertation

The thesis will be presented in the following manners:

In Chapter 2, synthesis procedure detail of liquid crystalline monomers and characterization is introduced. Then the fabrication method to construct film shape azo-LCEs actuator and Michael addition sequential thoil-ene reaction based onepot method procedure were explained. The details on each procedure were included.

In Chapter 3, contain experimental method for testing mechanical, optical, and thermal properties of azo-LCEs. The controlled detail and technics of property tests are also contained. And then, information of azo-LCEs came from Chapter 2 and Chapter 3 are follows. Methodology were basic actuation mechanism is investigated from both thermo-mechanical and polymer liquid crystal mesogen alignment aspects. The study on Michael addition sequential thoil-ene reaction based onepot method process was investigated.

In Chapter 4, key factors such as crosslinking density, initial preloadings force, and polymerization stage, which can alternate the photo-responsive actuation performance on azo-LCEs are investigated.

Chapter 5 contains the studies on mechanism, physics, and chemistry used in this dessertation. In this chapter, we will present deep understanding of reaction mechanism and study on catalyst on sequential polymerization.

Chapter 2. Synthesis and characterization

2.1 Synthesis of bi-acrylic azobenzene monomer

The two-step synthesis method (shown in **Figure 9**) of bi-acrylic functionalized azobenzene starts from commercially available 4,4'-(diazene-1,2-diyl)diphenol (DHAB, Tokyo Chemical Industry Co). K_2CO_3, 6-chlorohexan-1-ol, KI, $MgSO_4$, trimethylamine, acryloyl chloride, and hydroquinone were obtained from Sigma-Aldrich and used as received. Tetrahydrofuran (THF), *N*,*N*-dimethylformamide (DMF), chloroform, methanol, ethyl acetate, and deionized (DI) water were obtained from Daejung Chemical Co.

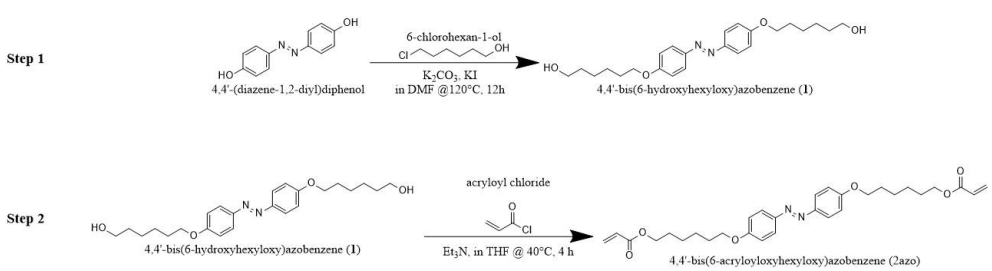

Figure 9. Synthesis scheme for the production of 2azo.

In the first step, 4,4'-(diazene-1,2-diyl)diphenol (2 mmol), 6-chlorohexan-1-ol (5 mmol), and K_2CO_3 (5 mmol) were dissolved in DMF (10 mL). A trace amount of KI was added as a catalyst to the mixture, which was refluxed at 120 °C for 18 h. After the reaction, the mixture was cooled to room temperature (25 °C) and 200 mL of water was added to fully terminate the reaction. Bright yellow precipitates were collected, dried overnight, and extracted by a THF–chloroform (1:1 v/v) solution. The organic layer was dried with $MgSO_4$ and recrystallized in a THF–methanol (5:4 v/v) solution to yield 4,4′-*bis*(6-hydroxyhexyloxy)azobenzene (**1**). The bright-yellow powder after crystallization were characterized by ^{1}H-NMR (shown in **Figure 10 a**) to confirm the full conversion of DHAB (yield: 96%).

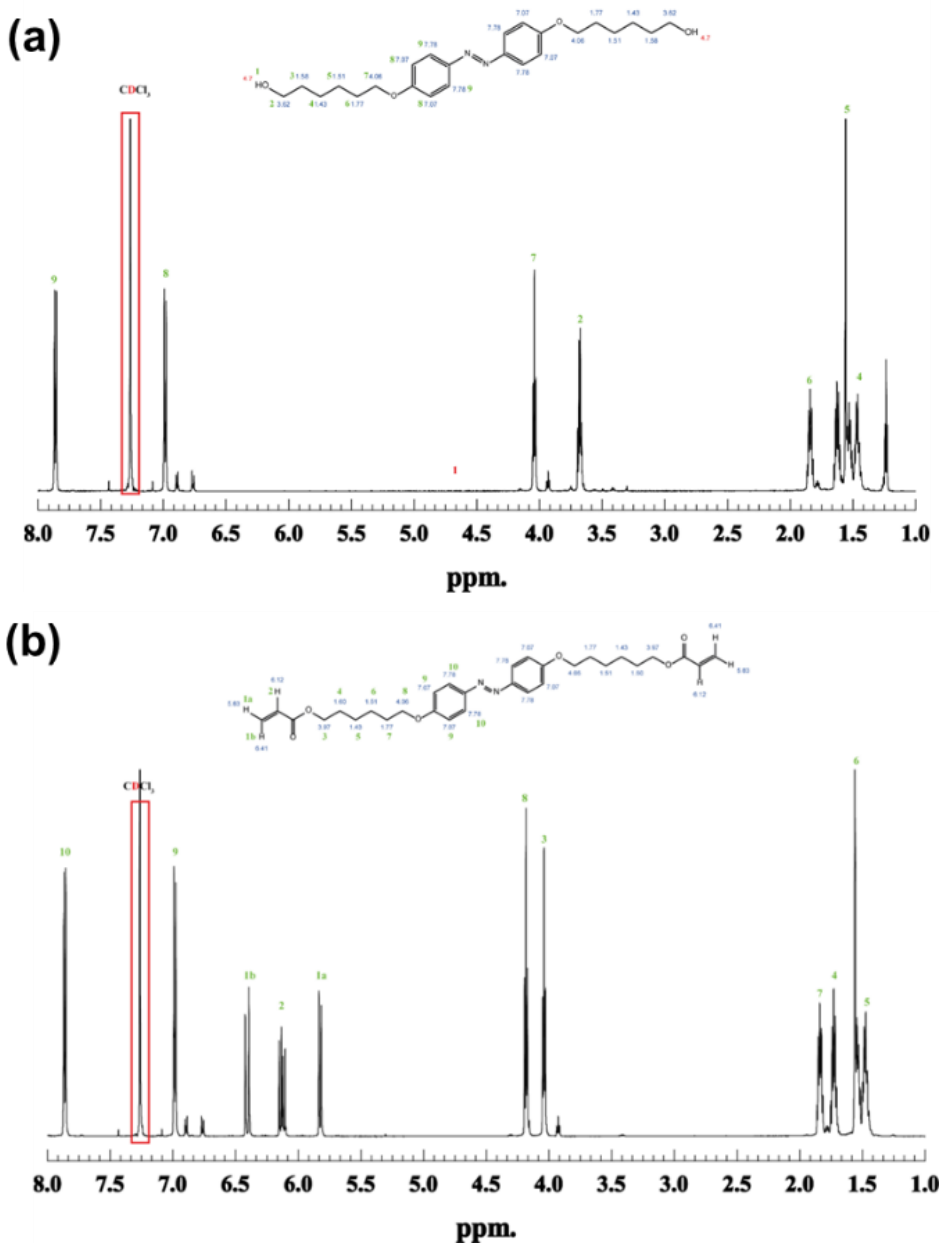

Figure 10. 600 MHz H^1-NMR spectra of (a) compound 4,4′-*bis*(6-hydroxyhexyloxy) azobenzene (1) and (b) 4,4'-bis(6-acryloyloxyhexyloxy)azobenzene (2azo).

In the second step, **1** (2 mmol), triethylamine (2 mmol), and acryloyl chloride (6 mmol) were dissolved in dehydrated THF (100 mL). A trace amount hydroquinone was dissolved to stabilize the self-polymerization. The solution was mixed at 0 ℃ for 4 h and then at 40 °C for 24 h. The reaction was quenched by pouring 500 mL of DI water into the mixture, after which it was extracted with chloroform several times. The organic phase was then dried with $MgSO_4$. After filtration, the extracted solution was condensed and purified by silica gel column chromatography (eluent/chloroform:ethyl acetate = 1:1, v:v). The resulting material was recrystallized in methanol to yield pure 4,4'-bis(6-acryloyloxyhexyloxy)azobenzene (2azo, yield: 66%). ^{1}H-NMR (**Figure 10b**, 600 MHz, $CDCl_3$): δ = 7.86 (dd, 4H), 6.98 (dd, 4H), 6.42 (d, 2H), 6.13 (dd, 2H), 5.82 (dd, 2H), 4.18 (t, 4H), 4.04 (t, 4H), 1.84 (m, 4H), 1.73 (m, 4H), 1.5 (m, 8H).

2.2 Synthesis of unsymetric-functionalized azobenzene monomer

Synthesis of 4-((4-(allyloxy)phenyl)diazenyl)benzoic acid (1).

4-(4-hydroxy-phenylazo)benzoic acid (2.4 g, 10 mmol) and K2CO3 (5.52 g, 40 mmol) was dissolved in 30 ml DMF. The mixture was thoroughly mixed for 1 hour at 80 ˚C before allyl bromide (3.6 ml, 40 mmol) was added. The suspension was further reacted for 5 hours at 80 ˚C and poured into 200 ml DI water. The mixture was extracted with EtOAc (50 ml *2) and the organic layer was washed thoroughly with aqueous NaHCO3 solution and dried over anhydrous MgSO4. After evaporation of the solvent, the intermediate was dissolved in MeOH/H_2O mixture with KOH (2.3 g, 40 mmol) and refluxed for 5 hours. After the reaction, methanol was evaporated from the mixture and the remaining solution was acidified by 1N HCl until pH is less than 3. The precipitates were collected and washed several times with DI water. The crude product was recrystallized in acetic acid to yield the target product. (yield: 2.03 g, 72%) ^{1}H NMR (500 MHz, Chloroform-*d*) δ 8.22 (d, *J* = 8.6 Hz, 2H), 8.00 – 7.90 (m, 4H), 7.05 (d, *J* = 9.0 Hz, 2H), 6.15 – 6.03 (m, 1H), 5.46 (dq, *J* = 17.3, 1.5 Hz, 1H), 5.35 (dq, *J* = 10.5, 1.4 Hz, 1H), 4.65 (dt, *J* = 5.3, 1.6 Hz, 2H).

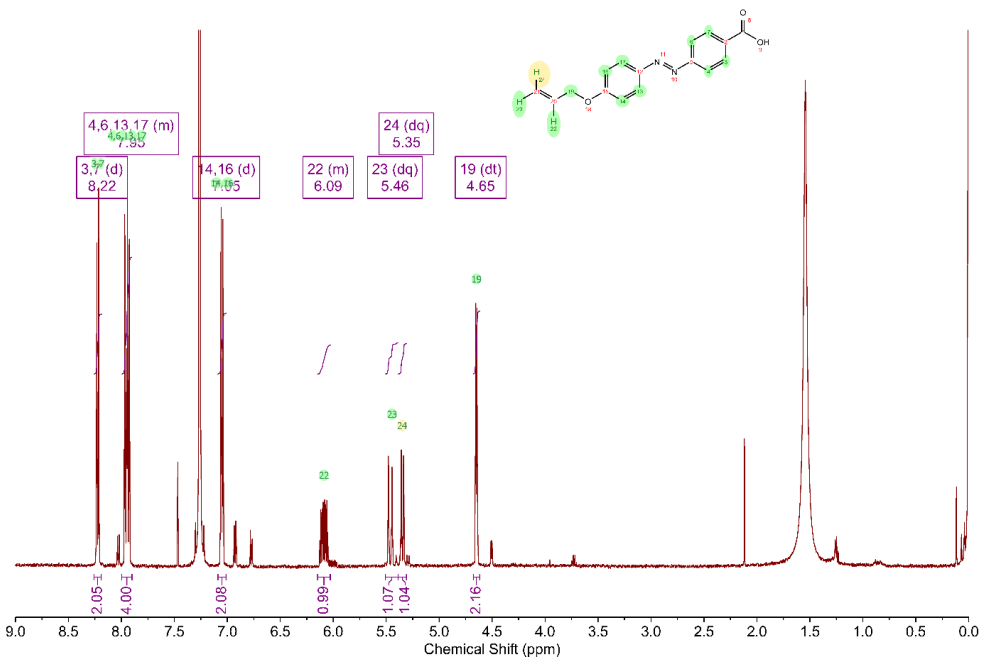

Figure 11. 500MHz ^{1}H-NMR spectra of 4-((4-(allyloxy)phenyl)diazenyl)benzoic acid (5 wt% in Chloroform-*d*).

Synthesis of 3-hydroxypropyl 4-((4-(allyloxy)phenyl) diazenyl)benzoate (2).

Product **1** (1.4 g, 5 mmol) and 1,8-diazabicyclo[5.4.0]undec-7-ene (DBU, 0.9 ml, 6 mmol) was thoroughly mixed in DMF (10 ml) for 1 hour before 3-chloro-1-propanol (0.52 ml, 6 mmol) was added. The mixture was then reacted at 120 ˚C for 5 hours. After the reaction, the mixture was poured into 100 ml DI water and extracted with DCM (50 ml *2). The organic layer was washed thoroughly with aqueous NaHCO3 solution and dried over anhydrous MgSO4. After evaporating the solvent, the crude product was purified by recrystallization in methanol to give the target product. (yield: 1.15 g, 69%) ^{1}H NMR (500 MHz, Chloroform-*d*) δ 8.17 (d, *J* = 8.6 Hz, 2H), 8.00 – 7.86 (m, 4H), 7.03 (d, *J* = 9.0 Hz, 2H), 6.14 – 6.02 (m, 1H), 5.46 (dq, *J* = 17.2, 1.6 Hz, 1H), 5.34 (dq, *J* = 10.5, 1.4 Hz, 1H), 4.64 (dt, *J* = 5.3, 1.6 Hz, 2H), 4.53 (t, *J* = 6.1 Hz, 2H), 3.81 (q, *J* = 5.5 Hz, 2H), 2.04 (p, *J* = 6.1 Hz, 2H), 1.90 (s, 1H)

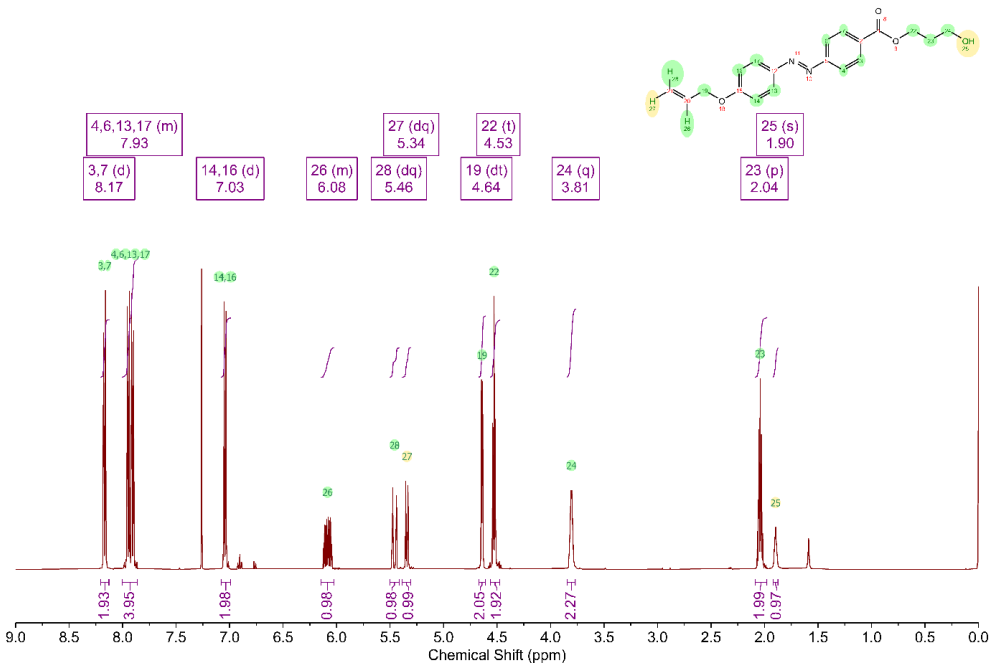

Figure 12. 500MHz ^{1}H-NMR spectra of 3-hydroxypropyl 4-((4-(allyloxy)phenyl) diazenyl)benzoate (5 wt% in Chloroform-*d*).

Synthesis of 3-(acryloyloxy)propyl 4-((4-(allyloxy) phenyl)diazenyl)benzoate (AB-azo).

Product 2 (1.36 g, 4 mmol), TEA (1.4 ml, 8 mmol) and trace amount of MEHQ was added to dry THF (20 ml) and cooled to 0 ˚C. A mixture of acryloyl chloride (0.65 ml, 8 mmol) in THF (10 ml) was added dropwise to the suspension. After stirring for 1 hour under argon atmosphere, the reaction was left at room temperature for 12 hours before 200 ml aqueous NaHCO3 was poured into the reaction vessel. The resulted suspension was extracted with DCM (50 ml * 2) and the organic layer was washed with DI water and dried over MgSO4. After evaporation of the solvent, the crude product was purified by column chromatography (eluent: EtOAc: n-Hex = 1: 2, v/v) and recrystallized from MeOH to give the final orange crystal product. (yield: 0.98 g, 62%) ^{1}H NMR (500 MHz, Chloroform-*d*) δ 8.17 (d, *J* = 8.6 Hz, 2H), 8.00 – 7.86 (m, 4H), 7.04 (d, *J* = 9.0 Hz, 2H), 6.43 (dd, *J* = 17.3, 1.4 Hz, 1H), 6.18 – 6.03 (m, 2H), 5.84 (dd, *J* = 10.4, 1.4 Hz, 1H), 5.46 (dq, *J* = 17.3, 1.6 Hz, 1H), 5.34 (dq, *J* = 10.6, 1.4 Hz, 1H), 4.64 (dt, *J* = 5.3, 1.5 Hz, 2H), 4.47 (t, *J* = 6.3 Hz, 2H), 4.37 (t, *J* = 6.2 Hz, 2H), 2.20 (p, *J* = 6.3 Hz, 2H).

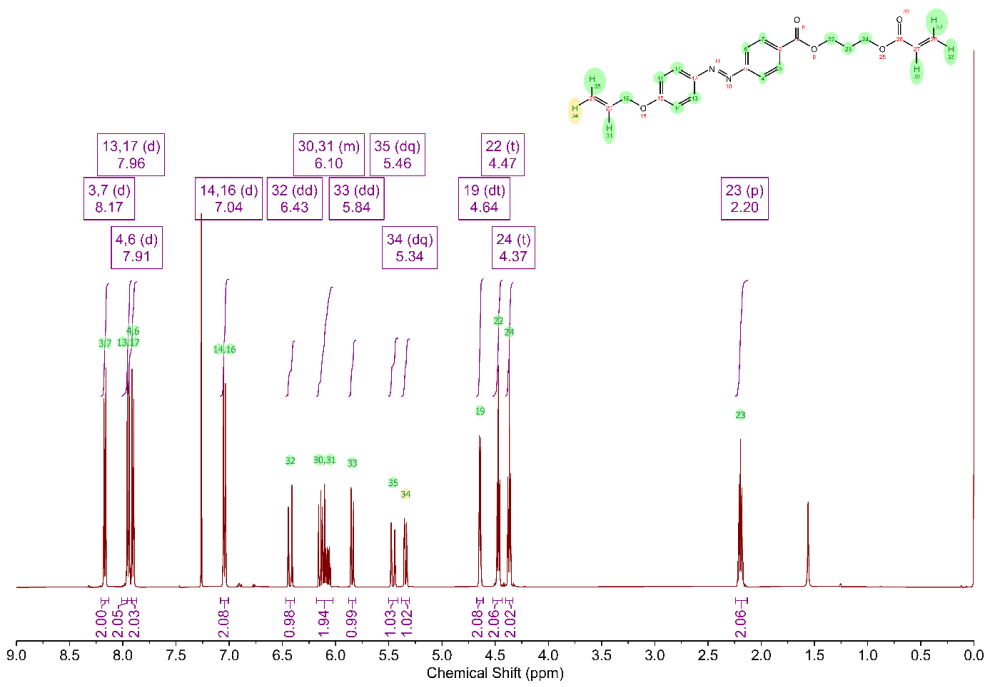

Figure 13. 500MHz ^{1}H-NMR spectra of 3-(acryloyloxy)propyl 4-((4-(allyloxy) phenyl)diazenyl)benzoate (5 wt% in Chloroform-*d*).

Synthesis of 3-hydroxypropyl 4-((4-(3-hydroxypropoxy)phenyl)diazenyl)benzoate (3).

4-(4-hydroxy-phenylazo) benzoic acid (4.8 g, 20 mmol), potassium iodide (KI, 9.96 g ,60 mmol), DBU (9 ml, 60 mmol) was mixed thoroughly in 40 ml DMF. 3-Chloro-1-propanol (60 mmol, 5.12 ml) was added dropwise into the mixtures and further mixed for 0.5 hour at room temperature. The reaction took place at 80 ˚C for 5 hours and terminated by adding 500 ml 0.1 M HCl solution. The resulted suspension was extracted with EtOAc (50 ml *3) and the organic layer was washed with DI water and dried over MgSO4. Finally, the solvent was evaporated, and the residuals are recrystallized twice from MeOH to give orange crystals (yield: 3.5 g, 50 %). ^{1}H NMR (500 MHz, Chloroform-*d*) δ 8.17 (d, *J* = 8.7 Hz, 2H), 7.96 (d, *J* = 9.1 Hz, 2H), 7.91 (d, *J* = 8.6 Hz, 2H), 7.04 (d, *J* = 9.1 Hz, 2H), 4.53 (t, *J* = 6.1 Hz, 2H), 4.23 (t, *J* = 6.0 Hz, 2H), 3.90 (s, 2H), 3.81 (s, 2H), 2.10 (p, *J* = 6.0 Hz, 2H), 2.04 (p, *J* = 6.1 Hz, 2H).

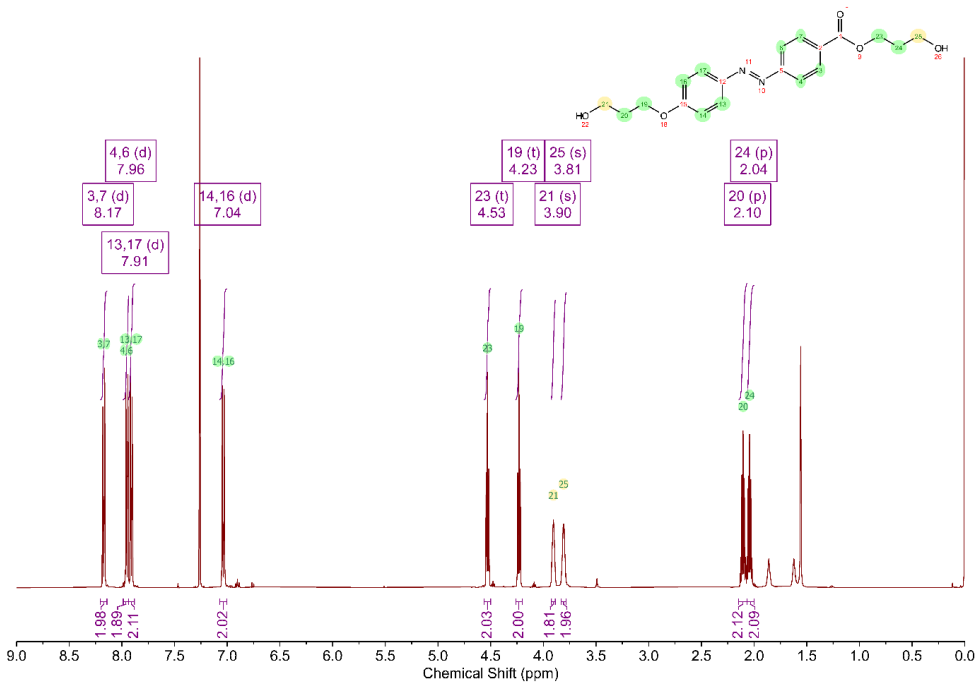

Figure 14. 500MHz ^{1}H-NMR spectra of 3-hydroxypropyl 4-((4-(3-hydroxypropoxy)phenyl)diazenyl)benzoate (5 wt% in Chloroform-*d*).

Synthesis of 3-(acryloyloxy)propyl 4-((4-(3-(acryloyloxy) propoxy)phenyl)diazenyl)benzoate (DA-azo).

This procedure is similar to the **AB-azo** synthesis procedure. The only difference is the amount of acryloyl chloride (3 molar equivalent of product **3**). The yield is 2.4 g (62 %) after purification. ^{1}H NMR (500 MHz, Chloroform-*d*) δ 8.17 (d, *J* = 8.7 Hz, 2H), 8.01 – 7.85 (m, 4H), 7.02 (d, *J* = 9.0 Hz, 2H), 6.43 (dt, *J* = 17.3, 1.2 Hz, 2H), 6.14 (ddd, *J* = 17.3, 10.4, 3.8 Hz, 2H), 5.85 (ddd, *J* = 10.4, 2.6, 1.5 Hz, 2H), 4.47 (t, *J* = 6.3 Hz, 2H), 4.38 (dt, *J* = 8.3, 6.3 Hz, 4H), 4.17 (t, *J* = 6.2 Hz, 2H), 2.21 (dp, *J* = 7.8, 6.2 Hz, 4H).

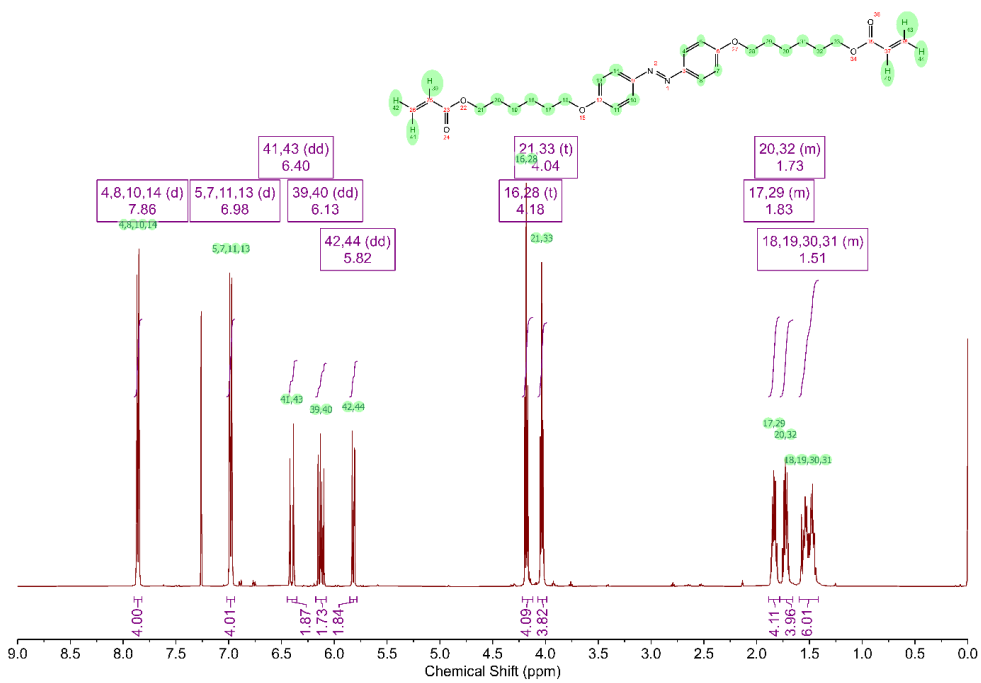

Figure 15. 500MHz ^{1}H-NMR spectra of 3-(acryloyloxy)propyl 4-((4-(3-(acryloyloxy) propoxy)phenyl)diazenyl)benzoate (5 wt% in Chloroform-*d*).

Synthesis of 4-allyloxyphenyl-4-allyloxybenzoate (APAB).

In a two neck round bottom flask, 11.512 g (50 mmol) 4-hydroxyphenyl-4-hydroxybenzoate, K2CO3 (130 mmol, 17.97 g) and trace amount of KI was refluxed in 100 ml acetone for 1 hour. Allyl bromide (150 ii, 12.7 ml) in 20 ml Acetone was then added into the suspension dropwise. After refluxing for another 48 hours under vigorous stirring the excessive solvent and allyl bromide was evaporated under vacuum. When the system cools to room temperature, DI water was poured into the flask and precipitations are collected by filtration. The crude product was recrystallized in methanol twice to give pure white target product (yield: 13.8 g, 89%). ^{1}H NMR (500 MHz, Chloroform-*d*) δ 8.14 (d, *J* = 9.0 Hz, 2H), 7.10 (d, *J* = 9.0 Hz, 2H), 6.99 (d, *J* = 8.9 Hz, 2H), 6.94 (d, *J* = 9.0 Hz, 2H), 6.07 (ddtd, *J* = 17.3, 10.6, 5.3, 2.7 Hz, 2H), 5.44 (ddq, *J* = 17.3, 9.9, 1.6 Hz, 2H), 5.32 (ddq, *J* = 18.9, 10.5, 1.4 Hz, 2H), 4.63 (dt, *J* = 5.2, 1.5 Hz, 2H), 4.54 (dt, *J* = 5.3, 1.5 Hz, 2H).

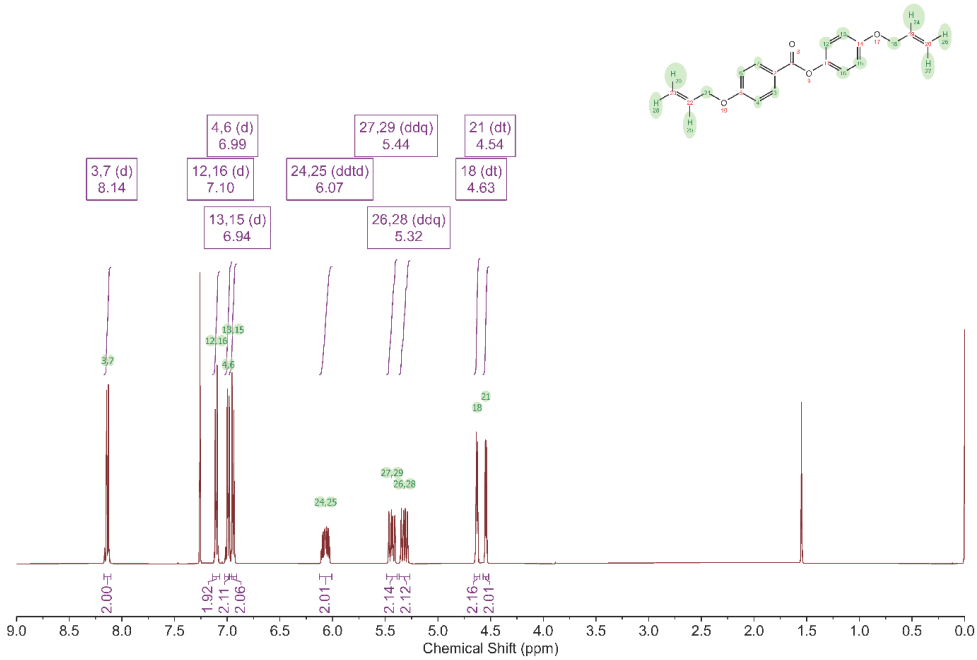

Figure 16. 500MHz ^{1}H-NMR spectra of 4-allyloxyphenyl-4-allyloxybenzoate (5 wt% in Chloroform-*d*).

2.3 Synthesis of azobenzene incorporated liquid crystalline elastomers (Azo-LCEs)

Acrylate liquid crystalline monomer: 4-(3-acryloyloxypropyloxy)-benzoic acid 2-methyl-1,4-phenylene ester(RM257), acrylate azobenzene monomer: 4,4'-bis(6-(acryoloxy)hexyloxy)azobenzene(2azo), thiol chain extender: 2,2'-(Ethylenedioxy)diethaneth(EDDET), thiol crosslinker:pentaerythritol tetrakis(3-mercaptopropionate) (PETMP) were formulated with specific ratio summarized in **Table 1**. The structure of each monomer is shown in **Figure 17**.

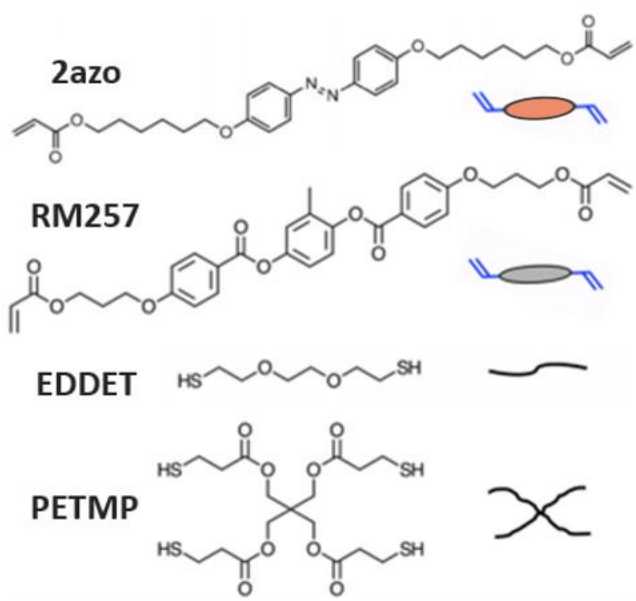

Figure 17. Scheme of chemical structures of the monomers.

Specific ratio of 2azo, and RM 257 were put in the 5ml vial with 0.2g of toluene. To fully melt the mixture, put vial on the hot plate with 80℃ during 5 minutes. When the mixture is fully change to the liquid state, put EDTET and PETMP into vial with specific ratio. The voltex mixer was used to make fully mixed compounds. 1 minute later after fully mix, put DPA with toluene into vial. DPA catalyst initiates michael addition thiol-ene polymerization between the acrylate reaction group and the thiol reaction group. After the DPA catalyst was put into the vial, polymerization is started very fast, so spread the liquid form mixture on the slide glass and spin coat the surface under the condition of 2000rpm. Before the polymerization, put the film sample into the vacuum pump to remove the air burbles inside the film. After the burble removing process, take film from the vacuum pump and give them about 30 minutes to partially polymerized. Now the film is a partially polymerized which means there are lots of unpolymerized reaction groups so it needs more time to fully polymerized and the initial shape in the room temperature condition is not fixed yet. After this process, the film sample is piled off on the slide glass and put into the vacuum condition with 80℃ during a day. In this step, the remaining unpolymerized part's polymerization is finished and we can design initial shape during this process. The initial shape created during this process is maintained under room temperature conditions, and exhibits shape memory effects for thermal and light stimulation. The

fully polymerized sample undergoes a swelling-deswelling process to remove uncrosslinked monomers remaining inside the molecule network. The samples were put into toluene during a day and put into vacuum oven with 80℃ during a day. In this process, residue monomers in the polymer were removed.

Table 1. Summary of the formulation ratio of the tested monomer compositions. Total molar amount of acrylate and thiol functional groups and the amount ratio between RM257 and 2azo were fixed to maintain the same condition while using various amounts of azobenzene.

Mole ratio (EDDET : PETMP)	RM 257	2azo	EDDET	PETMP
2 : 1	0.9	0.1	0.5	0.25
1 : 1	0.9	0.1	0.33	0.33
1 : 2	0.9	0.1	0.2	0.4

2.4 Onepot method based on two-step sequential thiol-ene reaction

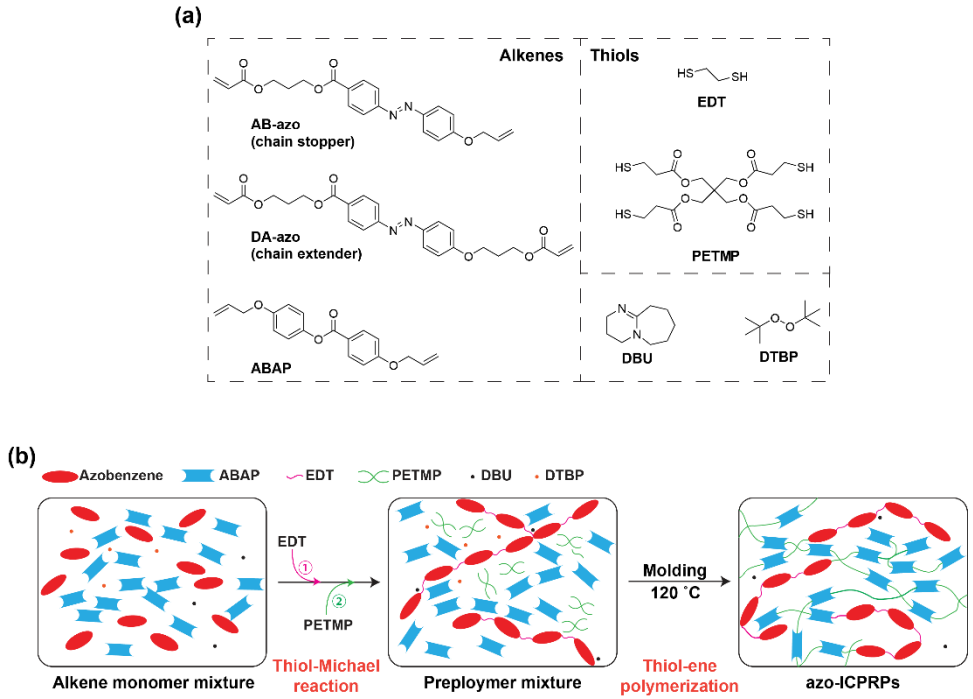

Figure 18. (a) Chemical structures of the materials used in this study. (b) Schematic illustration of two-stage synthesis method used in this study.

Materials

All the commercialized materials used in this study are purchased from Sigma Aldrich with the highest impurity and used without further purification unless stated otherwise. The thermal initiator Di-tert-butyl peroxide (DTBP, > 98%) was

purchased from Tokyo Chemical Industry. 4-hydroxyphenyl-4-hydroxy benzoate (> 98 %) was purchased from Alfa Chemistry. Glass cell coating agent "Ease release™ 200, Smooth-On, Inc." was degassed and diluted 5 times with n-hexane before the spin coating procedures. Tetrahydrofuran (THF), dimethylformamide (DMF), methanol (MeOH), dichloromethane (DCM), n-hexane (n-Hex) and ethyl acetate (EtOAc) were distilled and dried over activated molecular sieves (3 or 4 Å, Daejung Chemicals) for 48 hours before use. Acryloyl chloride (Wako, 97%) and allyl bromide (Alfa Chemistry, 99%) was distilled in dark and stored in amber vials 5 hours before use. The structure of monomers used in this study is shown in **Figure 18 a**. Synthesis procedures details of the monomers are provided in the *supporting information*. The glassware used in this section are cleaned and dried at 95 ˚C for 12 hours in a forced air convection oven before use.

Synthesis of the Azo-ICPRP thin films

The amount of 3-(acryloyloxy)propyl 4-((4-(allyloxy) phenyl)diazenyl)benzoate (AB-azo), 3-(acryloyloxy)propyl 4-((4-(3-(acryloyloxy) propoxy)phenyl)diazenyl)benzoate (DA-azo), 1,2-ethanedithiol (EDT), Pentaerythritol tetrakis(3-mercaptopropionate) (PETMP) and 4-allyloxyphenyl-4-allyloxybenzoate (APAB) are formulated with specific amount summarized in **Figure 18**. Here, we only provide the general procedure as illustrated in **Figure 18 b**.

Glass mold preparation

Glass slides was thoroughly washed by MeOH and DCM. The releasing agent in n-Hex is spin-casted on the glass slides at 4000 RMP for 30 seconds, which then dried at 100 ˚C for 5 minutes. The coated glass cells were placed and sealed together by an optical adhesive (NOA61, Norland) mixed with 40 μm PMMA microparticles (Fluka).

Preparation of reaction mixture and first step reaction

In a 5 ml amber vial, APAB (1 mmol) are thoroughly mixed by a micro magnetic bar with AB-azo and/or DA-azo in 0.5 ml chloroform for 0.5 hour. Amine catalyst (10 wt% in chloroform) is then added to the mixture and further agitated for 30 minutes at room temperature. The addition of thiol monomers in 1 ml chloroform are carried out by using the syringe (Norm-ject®, 1 ml) with bended needle plunged into the vial. The flow rate is controlled by a syringe pump (NE300, Newera) at 10 mL/hr. After the addition, the solution was left 3 hours at 65 ˚C for the total completion of the Michael addition reaction and removal of the solvent. The thermal initiator is added 5 mins before the vial was removed from the hot plate.

Molding and polymerization

The thiol-ene "click" reaction are not sensitive to atmosphere, therefore the reaction mixture can be easily molded into different shapes. However, polymerization between glass slides provide uniform thickness, which is beneficial for mechanical and performance tests. On the hot place with temperature set to 70 ˚C, the as-prepared mixture in the amber vial was melted and mixed for 5 minutes. The solution is then transferred to the glass molds and driven into the cell by capillary force. The cell was then polymerized at 100 ˚C for 3 hours and 130 ˚C for 12 hours. After opening the cell, the obtained elastomer was then placed in a hot oven (130 ˚C) under reduced pressure for another 24 hours to ensure total conversion.

Preparation of random co-polymer networks

The random co-polymer was prepared from the same method as the Azo-ICPRPs without the addition of any amine catalyst. Therefore, the monomer mixture was only polymerized by the free-radical mediated thiol-ene reaction.

Chapter 3. Methodology and sample properties

3.1 Experimental method for photo-actuation test of the azo-LCEs actuator

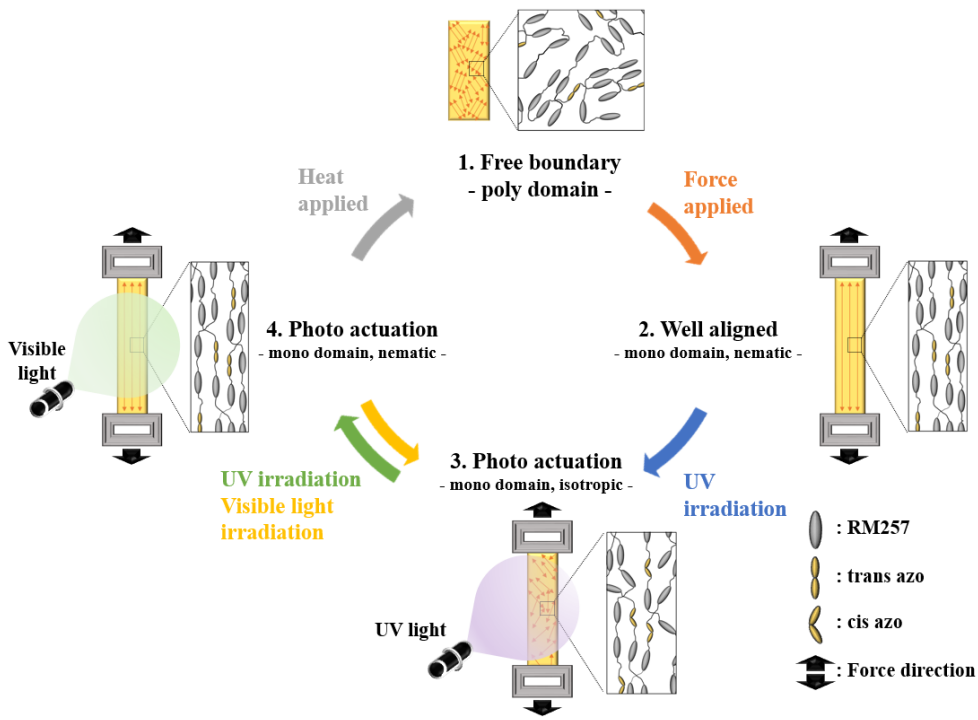

Figure 19. Scheme of the experimental system to measure the photo-actuation of azo-LCEs.

The azo-LCEs samples were tested by polarized light microscope and Dynamic Mechanical Analysis (DMA, Q800, TA instrument) to get mechanical and thermal properties such as glass transition temperature, nematic-isotropic phase transition temperature, young's modulus, and yield strain under the different sample conditions. The details of the experimental method are as follow.

Polarized optical microscopy (POM)

The formation of the film alignment under strain is confirmed by measured birefringence in cross-polarized optical microscopy (BX51P, Olympus).

Mechanical analysis

The thermomechanical analysis of the polymerized film is conducted on a DMA Q800 (TA Instruments). The storage modulus (E′) and glass transition temperature (T_g) are measured at a frequency of 1 Hz with temperature ramping (-40 to 60 °C, 3 °C/min). Rubbery modulus (E_r) is determined from the measured storage modulus at T_g + 10 °C. Stress-stain relationship is measured under a strain-ramping model at 2 % per minute. The crosslinking density is calculated from the famous Flory's rubbery theory following the equation:

$$v_e = \frac{E_r}{3RT_r}$$

where $T_r = T_g + 10\ °C$ is the starting temperature for the rubbery region, R is the idea gas constant.

Photo-actuation characterization

The samples for testing the photogenerated strain ($\Delta L/L_0$) are prepared by cutting the freestanding elastomer films into strips (20 mm × 5 mm). After loaded with controlled force on the DMA, the samples are allowed to relax for 20 minutes before any photo-irradiation after applied the pre loading force to align at room temperature. The collimated 365 and 530 nm LED (LCS-0365 and LCS-530, Mightex) are used to initiate and recover the photo isomerization of azobenzene. In a typical repeated procedure, the relaxed film is first exposed with 365 nm irradiation (15 mW/cm^2) for 10 minutes and then recovered by 530 nm irradiation (80 mW/cm^2) for 10 minutes. Generally, this procedure is repeated for 50 times for each measured external force. The actuator specific work capacity is calculated through the equation:

$$\delta W = \frac{\Delta L}{L_0} \cdot \sigma_{load}$$

, in which ΔL is the measured length change, L_0 is the equilibrium length after applying the external loading (σ_{load}). The power density output is calculated by using equation

$$P = \frac{d\Delta L}{dt} \cdot \frac{\sigma_{load}}{\rho}$$

, where $\frac{d\Delta L}{dt}$ is the length change during each measured time step and ρ is the density of the synthesized polymer.

3.2 Experimental method for in-situ test of the azo-LCEs actuator

Figure 20. Scheme of the thermal properties observe system constructed with DMA and light source.

To better understand of thermal and mechanical properties change during the photo-isomerization, real time in-situ experimental test was conducted. DMA and light source were connected by using our home-made metal gear and 3d printed gear. The inside part of the DMA can endure high and low temperature, so metal was used to construct connection part. Experimental methods have been reported to measure and compare changes in physical properties before and after photo-isomerization. However, in order to directly measure the changes in thermal and mechanical properties while conducting photo-isomerization through light irradiation in real-time, it is necessary to construct a measurement system that did not exist before.

First, a light source that can perform UV light irradiation in real time inside the DMA is connected through a metal gear. After that, a repetitive tension of 1 Hz is applied through the DMA initial frequency test option, and the tangent delta, storage modulus and lose modulus values according to the temperature change are measured through the temperature increasing option. At this time, since the loading force has a great influence on the order parameter of LCEs and the overall molecular structure, it is also possible to measure the effect of the loading force. Therefore, we intend to investigate the actuation mechanism of azo-LCEs by real-time observation of photo-isomerization and changes in physical properties according to the applied loading force through the real-time in situ test method.

3.3Mechanical/ thermal properties of the azo-LCEs actuator

Table 2. Summary of the mechanical and thermal properties information of the azo-LCEs samples.

Mole ratio (EDDET : PETMP)	Young's modulus (MPa)	Phase transition region (%)	Yield strain (%)	T_g (℃)	T_{NI} (℃)	v_e
2 : 1	0.02 / 0.07	20 ~ 65	690	16	48	0.37
1 : 1	0.37 / 0.70	17 ~ 52	522	26	55	0.63
1 : 2	0.83/ 1.42	14 ~39	241	39	67	0.79

The chemical components and construction ratio show in Table 1. We formulate the three samples which have different component ratio between EDDET/PETMP. The amount of azobenzene was fixed at 10 mol% in all alkenes and 5 mol% in all reaction groups. When the ratio of linear crosslinker (EDDET) is increasing, the flexibility of molecule system is also increasing. Accordingly, the transition temperature decreases, the mechanical properties such as modulus decrease, and the yield strain value increases. In addition, as a characteristic of a liquid crystalline elastomers, when an external force is applied in an isotropic phase that does not have a specific directional orientation, the liquid crystal moities in the molecule network are arranged in the applied external force, and a phase transition to the nematic phase occurs. During this process, mechanical, thermal, and photonic properties of the actuator are completely changed. The transition temperature (glass transition temperature (T_g) and Nematic-isotropic temperature (Tni)) are tested by DMA with temperature ramping mode and 1hz/s initial frequency mode. Young's modulus, and Isotropic/Nematic change range were tested by DMA with strain ramping mode. The yield strain of each sample were tested by strain machine. The property information shows in **Table 2** and each value is an average value of three samples produced under the corresponding condition.

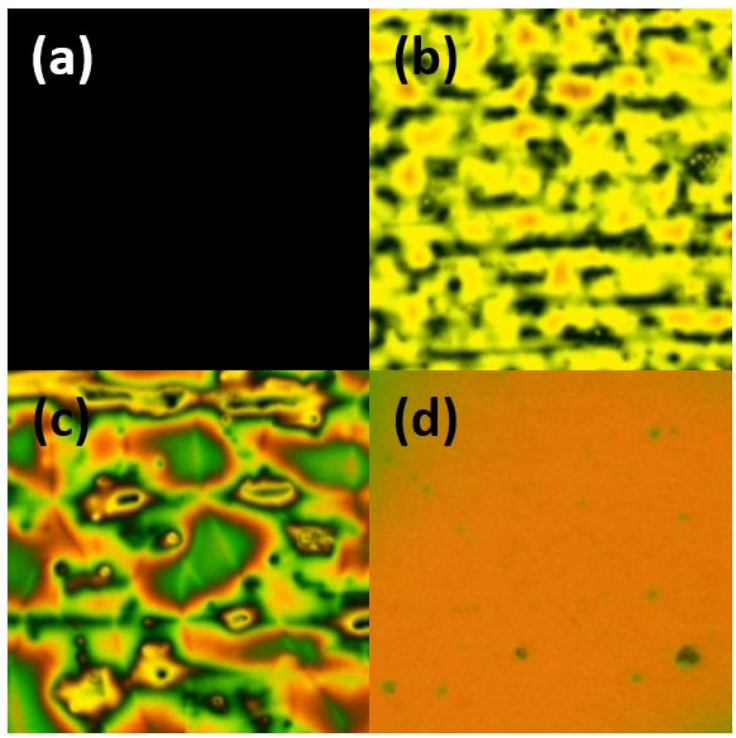

Figure 8. In-situ picture of POM. The sample were heated by heat controller from 20℃ to 60℃. The increasing speed is 2℃ per min. Each picture shows phase transition at a) 30℃, b) 40℃, c) 50℃, and d) 60℃. (T_g and T_{NI} of the sample are 22℃ and 55℃ each.)

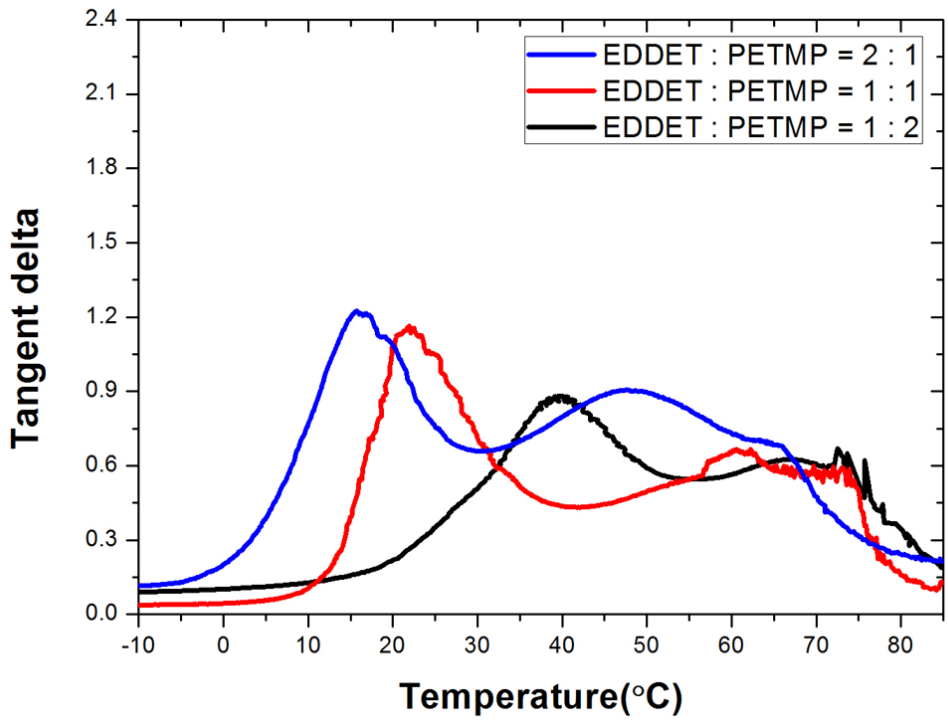

Figure 9. Three azo-LCEs samples with different crosslinking density were test by DMA. The temperature ramp mode was used without any force.

3.4 Controlled polymerization effect on properties of azo-LCEs

With the knowledge of reaction kinetics and catalyst selection, we then seek to control the Mn of azo-prepolymer by tuning the ratio between azobenzene chain extenders and stoppers. **Table 3** shows the composition of the tested monomer compositions. We keep a constant total azobenzene molar ratio with AB-azo concentration was tuned from 100 mol% to 0 mol%. GPC results demonstrate that there has been a steady drop in the Mn of the azobenzene oligomer as more chain stopper added into the monomer mixture. The Mn of oligomer could be tuned from 36400 g/mol to 840 g/mol (azo-EDT dimer). To our surprise, all the tested cases have shown the existence of dimers and the ratio of these azo-dimers deceases as less AB-azo added into the mixture. Because of the formation of stable dimers, unexpected octamers or higher molecular weight prepolymer are also detected in HeAB_2 and HeAB_4 samples. The theoretical value of Mn was estimated by using a step-polymerization model, in which the molecular weight can be expressed as

$$M_n = M_{eg} + \frac{M_0}{1 - p}$$

, in which p represents the extent of acrylate conversion; Meg is the molecular weight of the ending groups and defined as $2M_{AB-azo} - 2M_{DA-azo} - M_{EDT}$; M_0 is the molecular weight of the structural unit and defined as $M_{DA-azo} + M_{EDT}$. As shown, the theoretical Mn for full acrylate conversion (p = 1) agrees well with the measured azo-prepolymer Mn with the only exceptional HeAB_M case. This is probably due to the greatly decreased chain mobility at high Mn azo-prepolymer, which can dramatically decrease the reaction rate of the remaining EDT and acrylate groups.

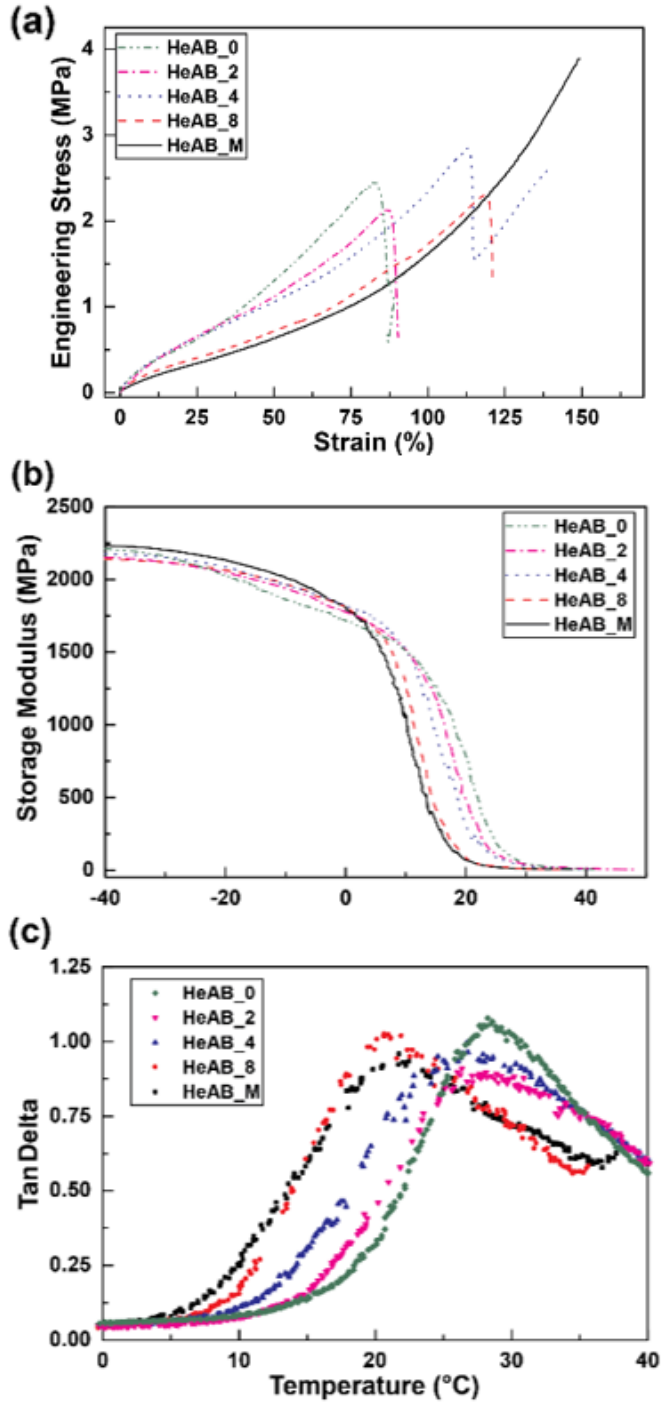

Figure 23. (a) Stress-strain relationship, (b) storage modulus (E') and (c) tangent delta (T_g) of the synthesized azo-ICPRPs.

After free-radical mediated thiol-ene polymerization, the dispersed azo-prepolymers are further reacted with the remaining monomers forming crosslinked networks. **Figure 23** and **Table 3** demonstrates the effect of azo-prepolymer M_n on the azo-ICPRP mechanical properties. In general, we have found the increase of azo-prepolymer M_n slightly decreases the elastic modulus at room temperature from 3 MPa to 1 MPa and the glass transition temperature (T_g) from 27.6 ˚C to 21 ˚C. Consequently, the crosslinking density (v_e) also decreases from 0.89 to 0.5 mol dm^{-3}. These results may be explained by the fact that DA-azo have longer flexible chains comparing to AB-azo, which can lead to higher monomers spacing. On the other hand, the azo-prepolymer M_n was found significantly enhancing the maximum strain and stress. Noticeably, the maximum strain of HeAB_M shows 150%, which is almost 2 times larger than the HeAB_0.

Table 3. Summary of the chemical formulation of the tested monomer compositions, GPC characterized azo-prepolymer chain after thiol-Michael reaction and DMA characterized polymer properties after second-stage free-radical mediated thiol-allyl polymerization.

Formulation Name	Monomer (mmol)				
	AB-azo	DA-azo	APAB	EDT	PETMP
HeAB_0	0.25	0	1	0.25	0.5
HeAB_2	0.125	0.125	1	0.25	0.5
HeAB_4	0.084	0.167	1	0.25	0.5
HeAB_8	0.05	0.2	1	0.25	0.5
HeAB_M	0	0.25	1	0.25	0.5

Azo-prepolymer properties		Elastomer mechanical properties		
M_n (g/mol)	DPI	T_g (˚C)	Rubbery modulus (MPa)	v_e (mol/dm^3)
840	1.03	28.24	6.7	0.89
2500	1.56	27.1	5.4	0.72
3800	1.64	26.41	4.79	0.64
6000	1.77	20.71	3.4	0.46
36400	2.12	21.3	3.69	0.50

Chapter 4. Photo-triggered actuation of the azo-LCEs based actuator

4.1 Characteristics of the actuation

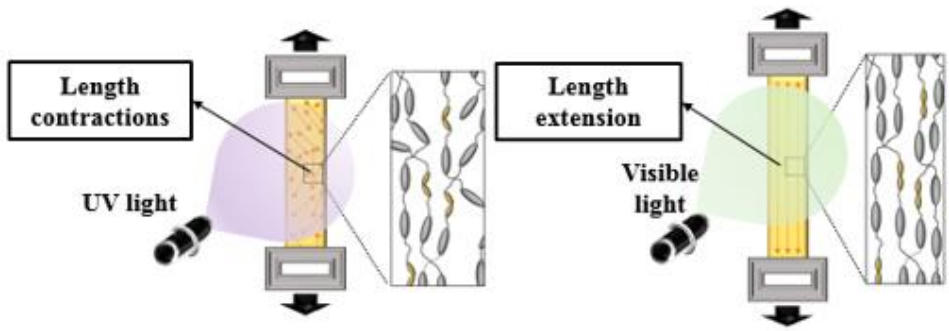

Figure 24. Scheme of photo responsive actuation of azo-LCEs and the molecule network system by each deformation step.

Azo-LCEs containing azobenzene in the molecule structure system are changed due to photo-isomerization of azobenzene moities when light of a specific wavelength is irradiated. UV light changes the state of azobenzene from trans to cis state, and visible light causes the opposite change, and this photo-isomerization affects the entire molecule structure network. In particular, in the case of LCEs, the mechanical properties are not strong, flexible, and the deformation rate is large.

If alignment is made through the process of applying a loading force to the cross-linked azo-LCEs sample, an order is created in the molecule structure in the direction of the loading force, resulting in a temporary increase in length. After that, when photo-isomerization of azobenzene is generated through light irradiation, not only the shape change of azobenzene itself, but also the surrounding molecular structures are affected, resulting in length contraction in the alignment direction. Conversely, when light in the visible light region is irradiated, azobenzene in the cis state returns to the trans state, restoring the existing length and alignment.

In addition to these deformation aspects, the molecular structure system becomes unstable, resulting in a decrease in mechanical properties and changes in thermal properties. This will be reported through experimental tests in a later chapter. Also, in the aspect that deformation occurs under loading force, it can be seen that this suggests a possibility as an actuator rather than a simple morphing. Until now, studies on sensors and actuators that operate through various triggers such as thermal, PH and humidity have been actively conducted, but there are still few cases of photo-responsive polymer-based actuator materials that can be controlled remotely. Azo-LCEs are capable of remote control, generate large deformation, and have the characteristics that the process is reversible, so the properties and behavior of Azo-LCEs will be introduced in the chapters to be introduced.

4.2 Effect of crosslinking density under the loading condition change

The azo-LCEs-based actuator is complexly affected by various factors such as light intensity and operating temperature irradiated during actuation, and in particular, the crosslinking density and applied loading force are the most dominant factors on the photo responsive actuation of azo-LCEs. The crosslinking density can be controlled by change of the ratio between thiol crosslinker EDDET and PETMP.

Changes in the ratio of crosslinking agent and preloading force determine the performance of actuators, such as the amount of deformation and work-output during actuation. In terms of the composition ratio of the thiol crosslinker, if the ratio of the linear shape thiol cross linker EDDET and the cross shape thiol cross linker agent PETMP is changed, the domain agglomeration of the liquid crystal moities inside the molecular arrangement is changes. Accordingly, the degree of change in the molecular arrangement of elastomers according to photo actuation, thermal actuation, and loading force also varies.

This is confirmed through the transition temperature result confirmed through the POM test result and the mechanical property result through the DMA test, and further acts as a decisive factor in the photo-actuating result under the pre-loading condition. To better understand, photo-strain actuation was confirmed under the intensity of preloading force was changed for three samples with different composition ratios of thiol crosslinkers EDDET and PETMP. The ratio of LC host monomer (RM257) to azobenzene monomer of azo-LCEs was fixed. Photo-actuation test under the pre-loading force is tested by experimental system constructed with DMA and UV/Visible light source. The azo-LCEs actuator samples are fixed by DMA under the each initial pre-loading force and after fully having a relaxation time, UV-light and Visible light are irradiated alternately to get a photo-actuation. The details of the experimental system shows in figure 2. The same light intensity (UV : 365nm, 15mW/cm^2, 530nm, Visible light : 80mW/cm^2) is used during test and each experimental process is under the same temperature condition (room temperature : 25C).

.

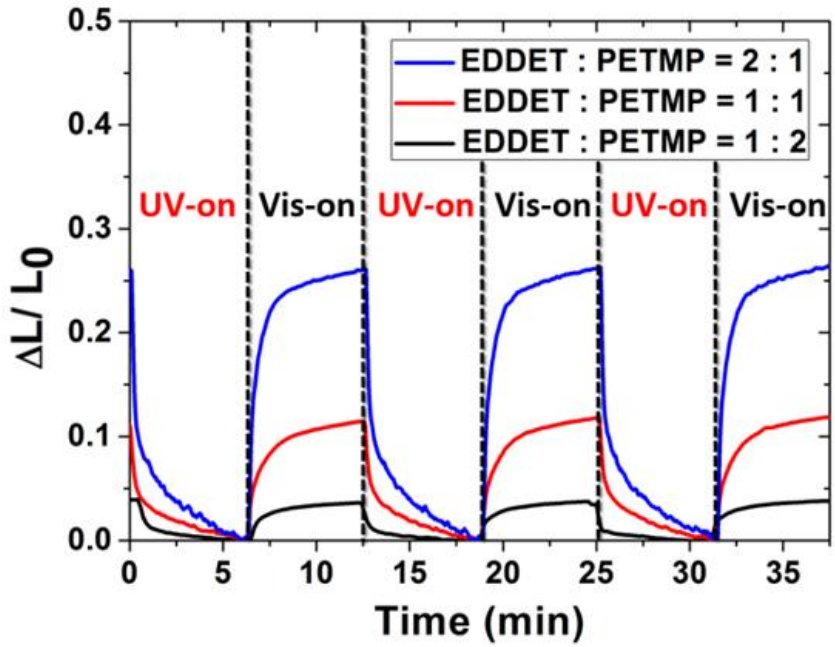

Figure 25. Photo-strain actuation of the azo-LCEs actuator. Comparison and confirm of the photo- actuation reversibility of each azo-LCEs. The external loading force is controlled and the actuations were measured under UV light (365nm, 15Mw cm-2) and visible green light (530nm, 80mWcm-2) irradiation. The test was tested under the fixed loading force of 0.05N.

Among the three types of azo-LCEs samples produced by us, samples 1 to 3 were named in the order of the highest EDDET composition ratio. The azo-LCEs actuators with three different thiol cross-linker composition ratios show significant differences not only in properties but also in photo-responsive actuation. The alignment given according to the external force direction, and a phase change occurs from isotropic to nematic. Because the mesogen inside the azo-LCEs changed to the nematic phase is arranged in the direction of an external force, the arrangement is disturbed by the photo isomerization of azobenzene according to UV irradiation, and photo-strain actuation occurs in the direction of the alignment. In this process, the crosslinking density of azo-LCEs has a dominant influence. When the ratio of EDDET increases, the crosslinking density decreases. Accordingly, the mechanical properties and transition temperature also decrease.

In particular, in the case of the sample1, the transition temperature value is about 10 degrees lower than the room temperature where the test was conducted, so it has very flexible properties. To test crosslinking density effect on photo actuation of the azo-LCEs, the 0.05N of loading force is applied and UV light and visible light were irradiated during 6min each. Photo actuation increasing is observed due to the crosslinking density increasing. From the result figure 4a), the sample1 shows overwhelmingly huge deformation. We started investigation from the viewpoint of the reason why sample 1 shows overwhelming actuation is effect of transition temperature shifting during photo-isomerization. It was confirmed that the room temperature, the temperature at which the test was conducted, is in the transition temperature change section before and after photo-isomerization of the sample1.

To know the preloading force effect in photo actuation of the azo-LCEs, the range of the applied force is needed. Each samples has a different stress which enough to make it fully mono domain and Nematic phase. These stresses can confirm at stress-strain curve of each samples. The smallest stress which comes from sample1 and the size of the stress is about 0.02MPa and the biggest stress which comes from sample3 and the size of the stress is about 0.05MPa. From this reason, the stress is controlled from 0.02N to yield point of the each sample. In all three samples, the strain increased up to each specific stress value and then gradually decreased past the maximum value. However, the degree is very different. In the case of sample 1 with a high EDDET ratio, it responds sensitively to changes in external force, and the change rate rapidly decreases with the increase in external force, but in the case of sample 3 with a low EDDET ratio, it was confirmed that almost no change in strain was observed. The result shows in **Figure 26**.

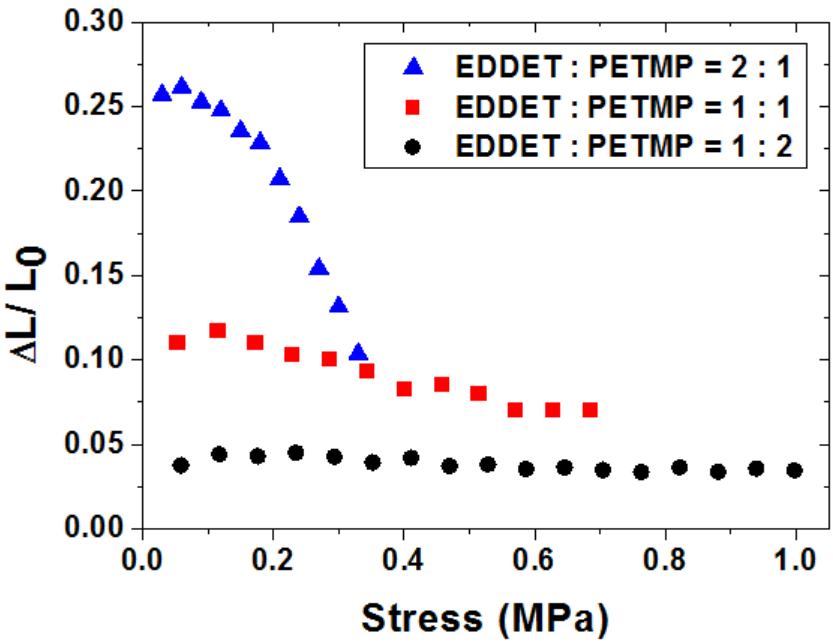

Figure 26. Photo-strain actuation of the azo-LCE actuator. Comparison and confirmation of actuations measured using UV light (365 nm, 15 mWcm-2) and visible green light (530 nm, 80 mWcm-2) irradiation under a controlled loading force. Tests a) and b) were performed at 25 ℃.

4.3 Effect of the sequential polymerization

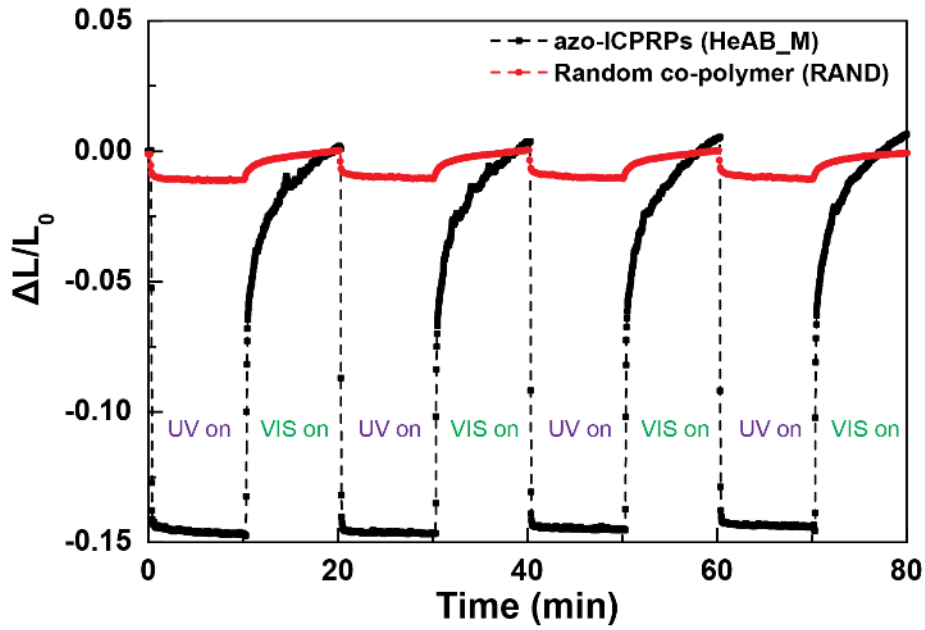

Figure 27. Comparison of photo-strain responses between the azo-ICPRPs (HeAB_M) and random co-polymers (RAND) at 0.3 MPa external loadings. Performance of the actuations were measured under the 365 nm (15 mW cm^{-2}) and 530 nm illumination (100 mW/cm^2) alternates every 10 mins on the samples (as indicated in the profile). RAND samples are prepared with identical monomer composite and procedure as HeAB_M samples, but without the addition of DBU. Dash lines are used to guild the eyes.

The effect of azobenzene interconnection on the actuation performances is studied by comparing the photo-strain kinetic profile of HeAB_M with traditional random co-polymers (RAND). For fair comparison, monomer compositions are set to identical in the tested samples with only HeAB_M samples adding the amine catalyst. Furthermore, we have limited the UV irradiation intensity to 15 mW/cm^2 to minimize the photothermal effect within 5 ˚C. Repeated UV-Visible light irradiations were used to test the reversibility of the samples under 0.3 MPa external loadings. The direct comparison of photo-strain kinetic profile between HeAB_M and RAND samples (shown in **Figure 27**) reveals striking difference in the maximum produced photo-strain. In HeAB_M samples, we have observed a reversible contracting actuation with more than 14.7 % shrinkage after each UV irradiation, while in RAND cases, only 1.2 % has been observed after 10 minutes of photo-actuation. Recall that the monomer composition between the tested samples are the same, the almost 10 times amplified photo-strain responses should be attributed to the azo-prepolymer resulted isomer interconnected structures.

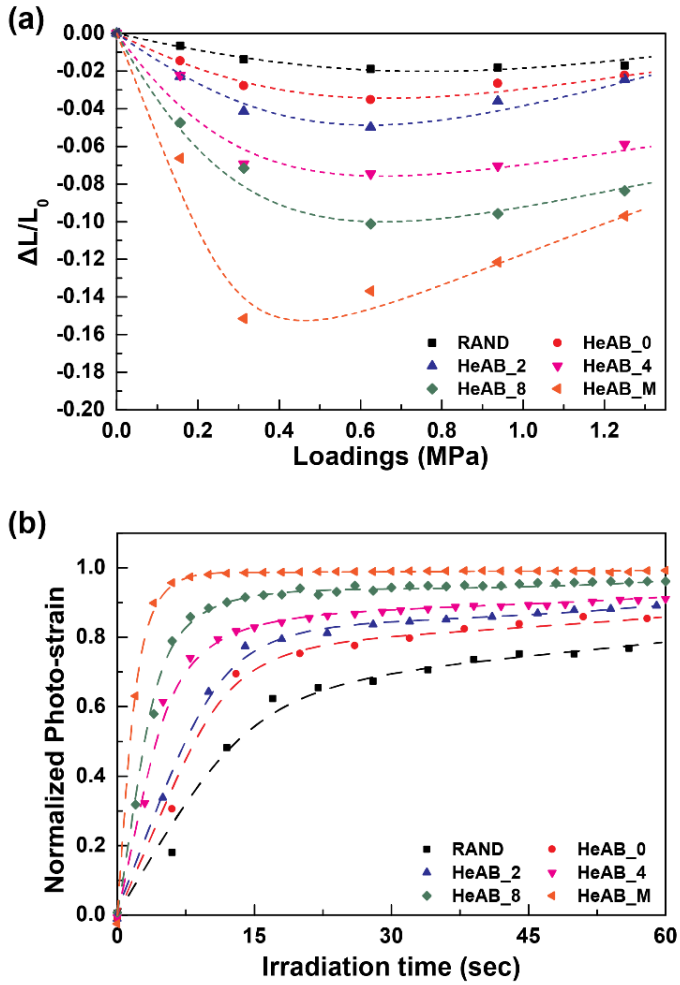

Figure 28. (a) The summarized average photo-strain responses and (b) normalized photo-strain kinetic profile of the azo-ICPRPs. For each prestress condition, the azo-ICPRPs were subjected to at least 4 illumination cycles, after which the averaged performance are summarized. The actuation conditions when azo-ICPRPs generate highest photo-strain are used to demonstrate the normalized photo-strain kinetics. Dash lines are used to guild the eyes.

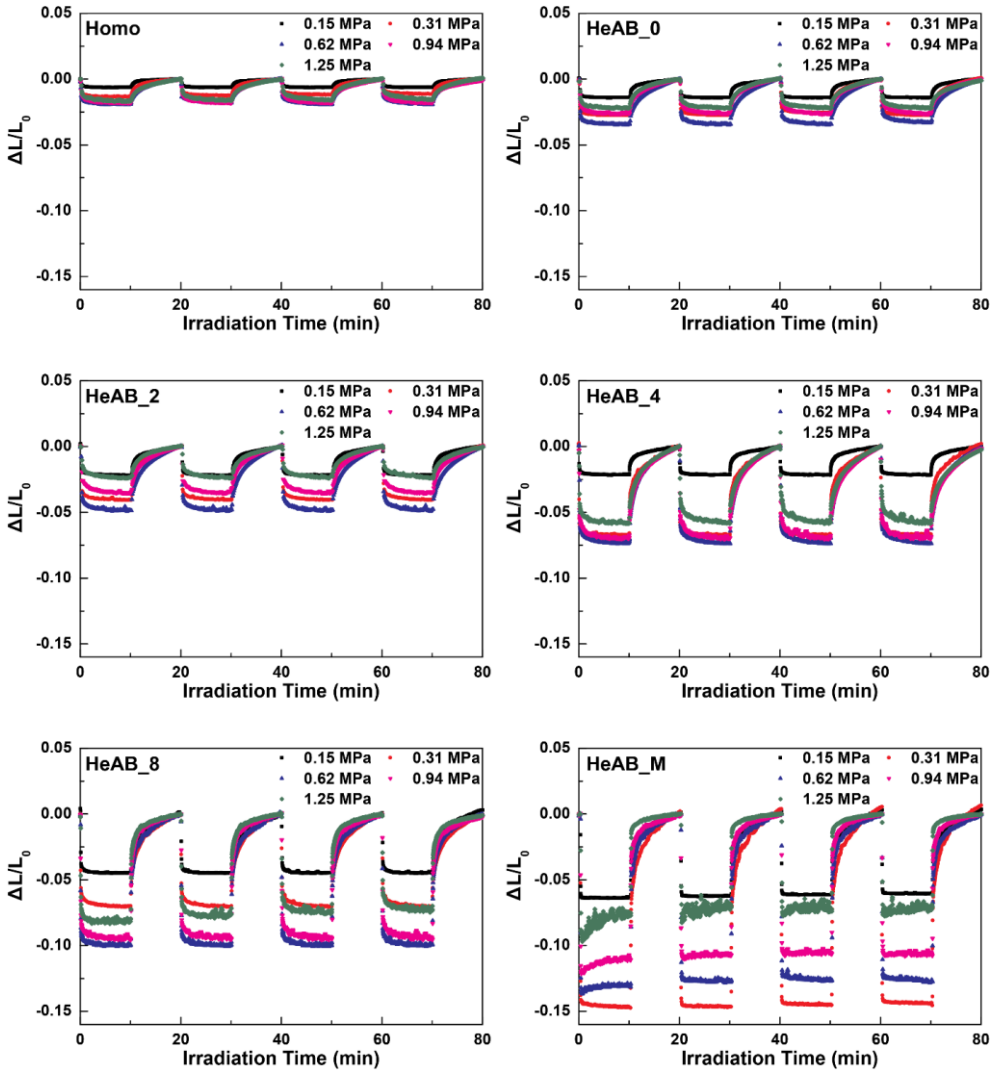

Figure 29. Photo-strain responses of the synthesized random co-polymers (RAND) and azo-ICPRPs. Performance of the actuations were measured under the 365 nm (15 mW/cm^2) and 530 nm illumination (80 mW/cm^2) alternates every 10 mins on the samples (as indicated in the profile).

4.4Azo-LCEs actuator as an artificial muscle

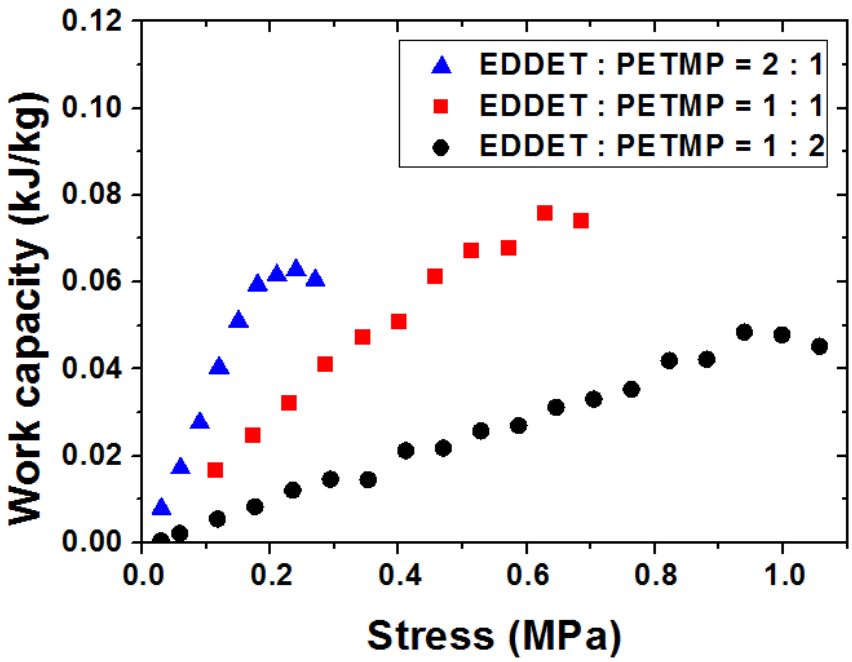

Figure 30. Photo-actuation work capacity between azo-LCEs under the changing loading force. Actuations measured using UV light (365 nm, 15 mW/cm^2) and visible green light (530 nm, 80 mW/cm^2) irradiation under a controlled loading force.

The work capacity change was measured under the external force change of the azo-LCEs samples. The each sample's stress conditions showing the maximum work capacity were different. Each sample showed the greatest work capacity value at 0.23 MPa, 0.62 MPa, and 0.94 MPa, and as the crosslinking density increased, the stress value that produced the maximum output and the stress value that could be tolerated increased as the crosslinking density increased. For example, sample 1 was the most flexible and showed the largest photo actuation, but it was found that the lowest yield stress values. However, the maximum work capacity value that each sample could produce did not show the same tendency as the crosslinking density. All samples had work capacity values that exceeded the work capacity of mammalian muscles. Especially sample 2 which showed the highest maximum work capacity, showed work capacity values that were more than twice that of mammalian muscles. As can be seen from the previous photo actuation test results, it was found that each sample had the most suitable operating environment. The experimental result shows in **Figure 30**.

Chapter 5. Actuation mechanism

5.1 Study of the catalyst

In this work, a two-step sequential reaction is used for the synthesis of azo-ICPRPs. Di-allyl functionalized monomer (APAB) and tertrathiol monomer (PETMP) is used as the embedding substrate since this combination offers great optical transparency (T > 75% at 365 nm in 75 μm films, ref to Figure S8a) and stable crosslinked polymer network. The dose of azobenzene are fixed at 20 mol% in the total amount alkenes, and 12.5 mol% in all monomers. The synthesized *trans*-state azobenzene monomers are found to have characteristic absorption peak at 360 nm owning to the $\pi \rightarrow \pi^*$ excitation with 2×10^4 M^{-1} cm^{-1} molar absorptivity in chloroform (ref to Figure S8b). Under 35 seconds of UV irradiation (2 mW/cm^2), *trans*-state DA-azo in chloroform can be fully converted into the *cis*-state.

Here, we would like to mention that the polymerized azo-ICPRPs are conventional elastomer instead of liquid crystalline polymer although APAB presents a nematic region from 88 to 49 ˚C. Therefore, the actuation of azo-ICPRPs requires external prestress/strains to form the initial polymer anisotropy. However, because this method requires absolutely no prerequisite polymerization conditions (e.g. electric/magnetic field, surface alignment and low oxygen content), it could be easily integrated into many manufacturing processes such as 3D printing techniques. Light distinguishes itself from the other means of programming and stimulations for actuators (e.g. electric field, heat, magnetic, solvents) from its capability of remote control and high energy input. Moreover, due to the easy control of the spatial intensity distribution as well as the polarizing characteristic of the electric-magnetic waves, light programming could offer much richer capability of controlling the patterns than other types of stimulations (shown in **Figure 31**). These characteristics have made photo-programming the main manufacturing methodology for the modern semi-conductor industry (e.g. photolithography, photo-depositions and *et. al*).

Orthogonality of the Thiol-acryloyl and Thiol-allyl reaction

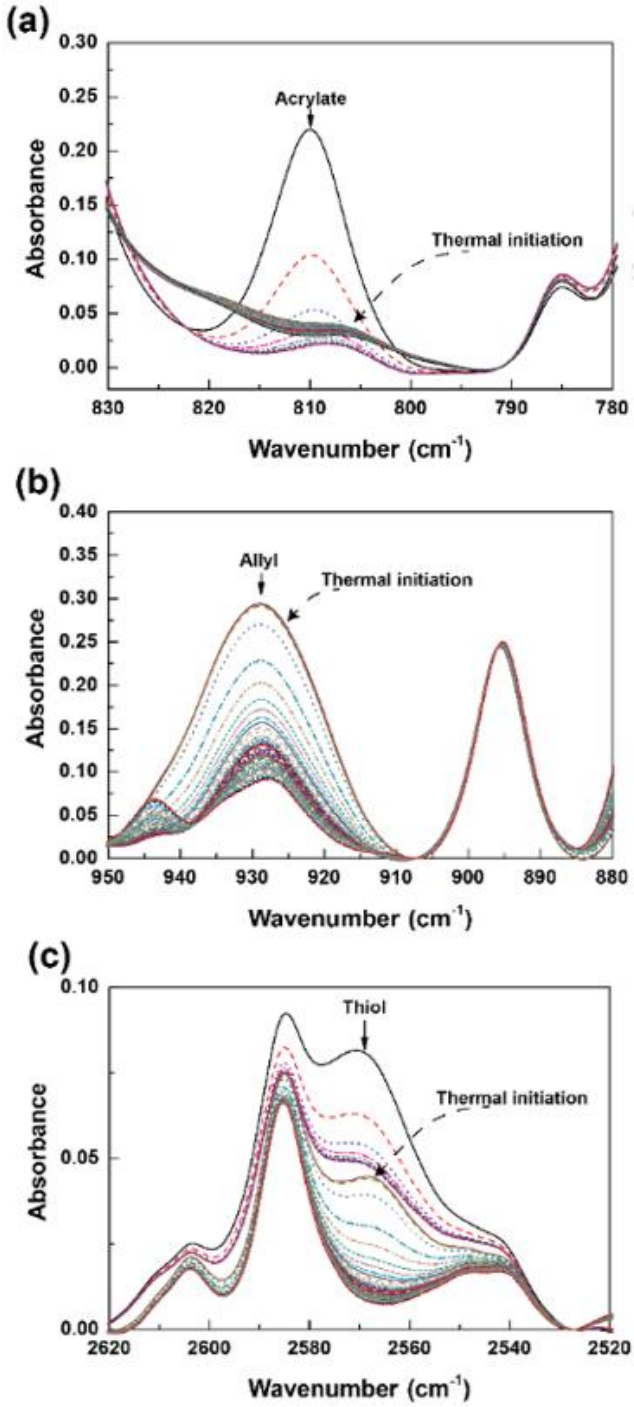

Figure 31. Real-time FTIR spectra of (a) thiol, (b) allyl and (c) acrylate functional groups during the two-step thiol-ene reaction. The monitored monomer mixture contains equal molar ration of AB-azo and EDT. DPA (0.2 mol%) was used to catalyze the thiol-Michael reaction. Free radical mediated thiol-allyl reaction was initiated at 100 ˚C with 1 mol% of DTBP. Spectra are only showed every 10 minutes for clear illustration, but during the thiol-Michael addition reaction the reaction was monitor every 20 seconds.

To verify the chemoselectivity of thiol-Michael reaction and thermal-initiated free-radical polymerization, real-time FT-IR spectrometer is used to monitor the reaction. To facilitate quantitative measurement, equal molar amount AB-azo and EDT was used as the reaction mixture. AB-azo is an asymmetric difunctionalized monomer with allyl groups and acryloyl groups on each side of azobenzene, therefore, it provides equal among of allyl and acryloyl groups in the mixture. Nucleophile amine catalyst (DPA, 0.2 mol%) and thermal initiator (DTBP, 1 mol%) is loaded into the mixture right before the measurement. Because the preparation process usually takes 5 seconds, the initial IR spectra of the mixture without catalyst was used as the data for 0 minutes. **Figure 32** summaries the time evolution of measured IR spectrum during both thiol-Michael addition and thiol-allyl reactions. From the presented data, one can observe a steep decline in the IR intensity of acrylate and thiol characteristic peaks at 810 cm^{-1} and 2570 cm^{-1}, evidencing acrylate and thiol groups reacts rapidly during the first step of the reaction.[46] After 80 mins of reaction, almost all the acrylate and half thiol reactive groups were reacted. More importantly, no significant differences were found in the IR absorbance of allyl groups at 930 cm^{-1} during this stage of reaction, meaning allyl groups remain unreacted during this step of the reaction.[47] During the second step reaction, both allyl and thiol were found reacted with each other after the thermal initiation. The strategy and methodology introduced

in this thesis takes both advantage of the light programming and the internal alignment programmability of azo-LCP systems, which provide immersive amount of possibilities to realize the designed actuations.

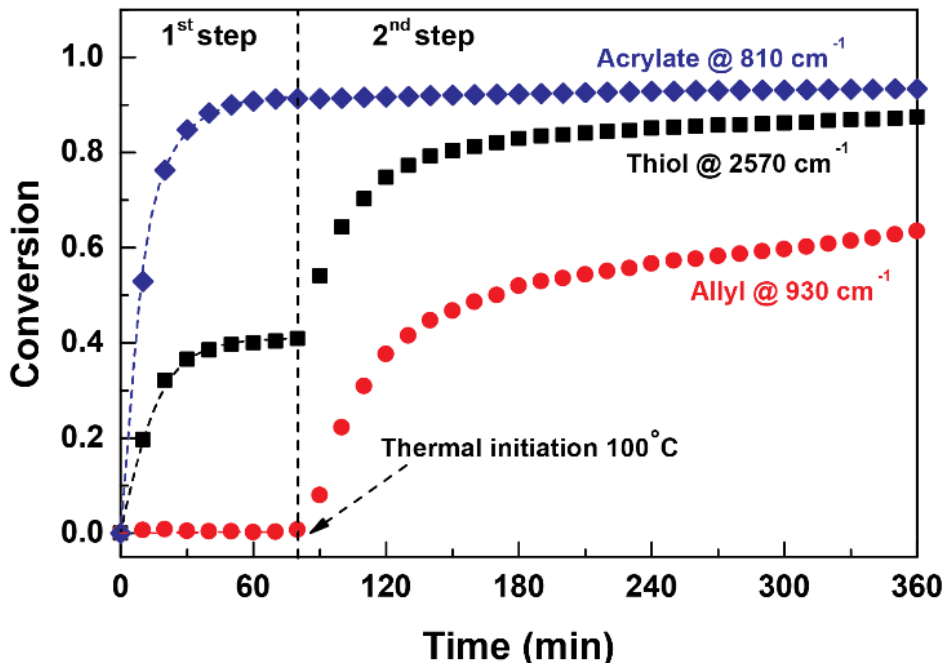

Figure 32. FTIR measured reaction kinetic profile of the two-step reaction. Functional group conversion is calculated from the characteristic peak intensity of each functional groups. Dashed line indicates the IR measured data collected every 20 seconds. The second step thiol-allyl reaction was measured every 10 minutes.

Figure 32 summaries the function group conversion measured from the IR spectrometer. The graph shows only 0.7 % of the allyl groups are converted while 44.7 % of the thiol and 91.2% acrylate groups are converted at the end of thiol-Michael reaction. The measured thiol/acrylate conversion ratio 2.04 fits well to the ideal value of 2, suggesting a great conversion efficiency and chemo-selectivity in the first step thiol-Michael reaction. After the thermal initiation, the remaining thiol reactive group starts to react with allyl group forming thiol-ethers. Comparing to the widely used photo-initiation process, the thermal initiation is found much slower because of the relatively high thermal stability of DTBP. After 280 mins of reaction at 100 ˚C, 87.43% of total thiol and 63.4 % of the allyl groups were reacted. The excess conversion of thiol could be attributed to thiol-acrylate reaction because there are still 9 % unreacted acrylate groups. After 360 minutes of the reaction, the measurement was terminated because the reaction mixture became too viscous to be measured in liquid cell. Despite of the current limitation of our observation, DTBP is proven to be an effective thermal initiator for high temperature initiating the thiol-ene "click" reaction. Here, we would like to point out the reason for not utilizing the conventional highly efficient photo initiator (e.g. Irgacure 819) in our study is because the extremely high UV-Blue absorption of the azobenzene moieties in the system will lead to a very shallow light penetration profile in the samples, resulting

in non-uniform polymerization in the thin film. The high temperature thermal initiator also provides long gelation time at moderate temperature for mold injection comparing to other low temperature initiators, such as AIBN or BPO, which is very important for the manufacture of thin film actuators.

Effect of catalyst selection on the reaction kinetics and azobenzene oligomerization

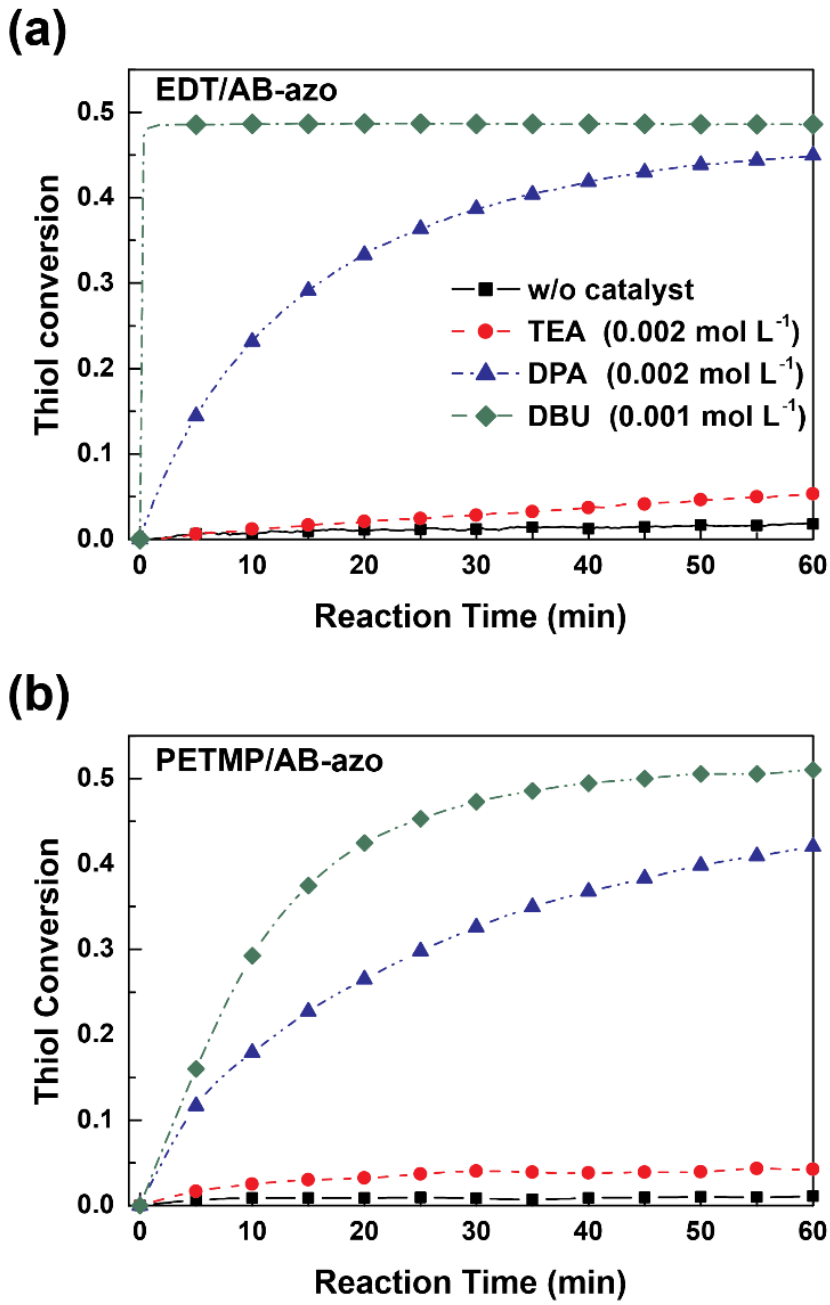

Figure 33. Kinetic profile of acrylate conversion during thiol-Michael reaction in the presence of three different amine catalyst: TEA, DPA and DBU. Each monomer mixture contains (a) equal amount of EDT and AB-azo (both 1 mol/ L) or (b) 0.5 mol/L of PETMP and 1 mol/L of AB-azo in toluene. The catalyst was added right before the test. Dashed line indicates the IR measured data collected every 20 seconds.

Earlier studies have revealed that the kinetics and completion of the thiol-Michael reaction depends on the selection of amine/nucleophile catalyst of thiol-Michael addition.[46] In our proposed method, successful synthesis of azo-prepolymers requires gradual thiol monomer addition to ensure the excessive amount of acrylate in the reaction mixture before full conversion. Therefore, fast reaction kinetics with high conversion ratio is preferred in order to avoid any possible partial reactions. Three types of widely used amine catalysts: TEA, DPA and DBU are tested to study the effect of catalyst selection on the kinetics of thiol-Michael reaction and the resulted molecular weight of the azo-prepolymers.

To measure the kinetic of the reaction, we use the same AB-azo/thiol mixture as the last section. **Figure 33** demonstrate the kinetics of thiol conversion profile during the Michael addition reaction in AB-azo/thiol systems and Table summaries the reaction constant (k_a) for the same formulations. From the demonstrated data, some characteristic trend can be observed: (i) Without the addition of catalyst, there are essentially no conversion of thiol (less than 1 %) even after 60 minutes of reaction at room temperature. (ii) For both thiol monomers (EDT and PETMP), the trend of catalytic activity follows the same order: TEA < DPA < DBU. Particularly, the k_a values of DBU are 2 orders of magnitude larger than DPA with only half concentration. (iii) Final conversion ratio of thiols also highly depends on the selection of catalyst. TEA can only catalyze the reaction with less than 5 % of the thiols converted at the end of the test, while DPA and DBU can achieve relatively high thiol conversion ratio. The final conversion of thiol reached to 44.9 % for EDT, 42.1% for PETMP in the case of DPA, while in the case of DBU, 48.6% for EDT and 49.7% for PETMP was observed. (iv) In terms of different thiol monomers, EDT presents much higher reaction rate than PETMP. This phenomenon is found most profound with the presence of DBU, where EDT reacts over 200 times faster than PETMP with AB-azo.

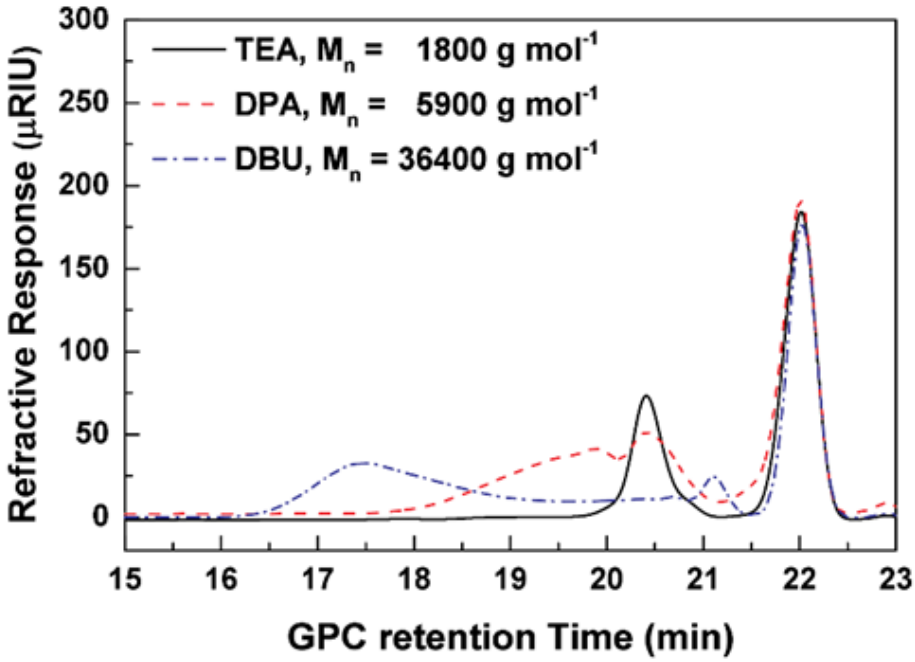

Figure 34. GPC traces spectra of HeAB_M monomer mixture catalyzed by DBU, DPA and TEA. To avoid any possible free-radical generation, thermal initiators are not added. After the first step reaction, the formed solids at room temperature was melted in THF (0.5 wt%) for the characterization.

To further study the effect of catalyst selection on azo-prepolymer molecular weight, HeAB_M mixtures (shown in **Figure 34**) catalyzed by different amine catalyst are characterized by GPC spectrometer. In theory, HeAB_M mixture can provide infinite long azo-prepolymer chain because the azobenzene moieties contain only DA-azo chain extenders. GPC measured molecular weight distributions (**Table 4**) suggest that the selection of amine catalyst have decisive effect on the number averaged molecular weight (M_n) of the azo-prepolymers. The M_n of azo-prepolymers are only 1800 and 5900 g/mol in the TEA and DPA catalyzed cases, which is much lower than the expected value. Furthermore, because the reaction rate EDT is much slower than the addition rate of thiol monomers, both cases were found to have high absorption signal around 2200 g/mol, which corresponding to the undesirable azo-PETMP oligomers. Meanwhile, DBU can successfully catalyst the reaction and synthesis high M_n azo-prepolymers. The measured M_n is 36400 g/mol, which contains up to 62 [EDT-azo] block units. More importantly, the disappearance of azo-PETMP oligomer peak signals suggests DA-azo have already been consumed by EDT forming polymer chain before the addition of PETMP monomers owning to the DBU catalyzed fast reaction kinetics.

Table 4. Apparent rate constant of thiol-Michael reaction with different types of amine catalyst and thiol monomers.

Catalyst	Amount of catalyst (mol%)	Reaction Constant ($k_a \times 10^{-4}$ mol/Ls)	
		EDT	PETMP
TEA	0.2	0.6	0.12
DPA	0.2	24.7	10.5
DBU	0.1	2420	34.7

5.2 Real time in-situ test to know the thermal properties change under the photo-isomerization

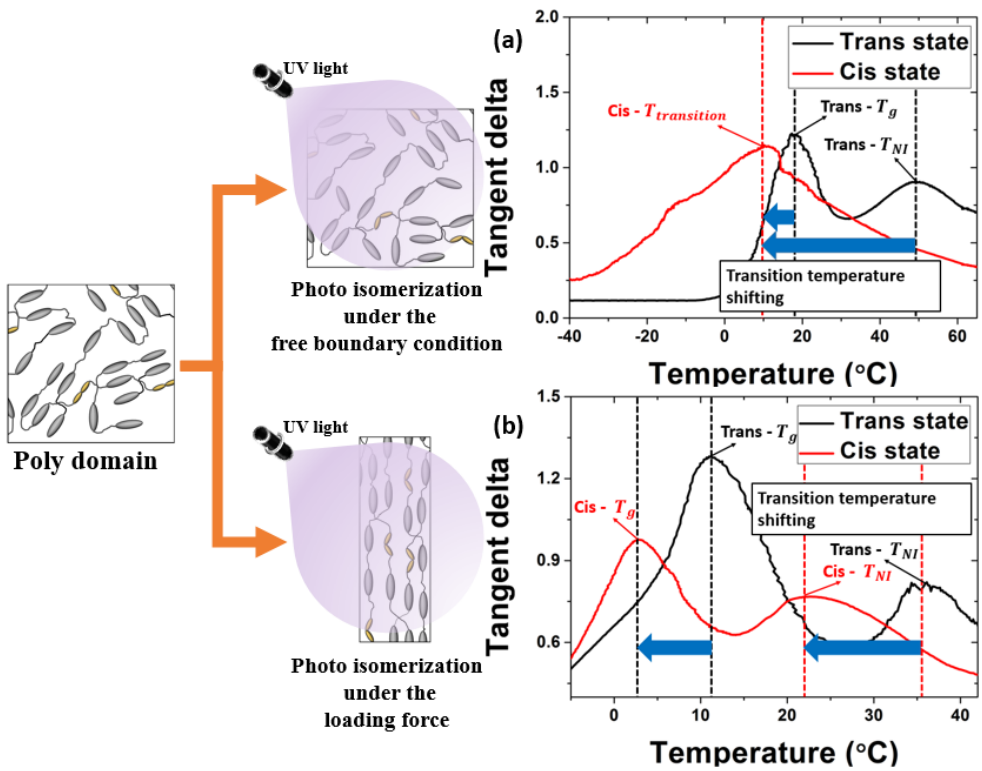

Figure 35. Comparison of a) transition temperature shifting of azo-LCEs due to the photo-isomerization under the free boundary condition and b) 0.05N of the loading force.

The change in the physical properties of azo-LCEs due to photo-isomerization of azobenzene was measured through the real-time insert test. At this time, the most decisive factor was the change in the degree of molecular arrangement of azo-LCEs according to the strength of the external force. When no external force is applied, azo-LCEs represent two tangent delta peaks: glass transition temperature and nematic-isotropic phase transition temperature, respectively. At this time, if photo-isomerization occurs due to UV radiation, the molecular arrangement change resulting from this will not be able to represent the nominal phase. Therefore, the two tangent delta peaks are combined into one, and the transition temperature decreases due to the photo softening effect. However, when a unidirectional loading force is applied, a forced orientation occurs according to the direction of the force, thereby offsetting the orientation distortion caused by photo-isomerization. Therefore, it has two peaks as under the free boundary condition. Therefore, it maintains the tendency of the existing tangent delta and shows transition temperature shifting by photo softening. At this time, the magnitude of the loading force sufficient to make the nematic phase can be obtained through the DMA strain test. Like general unordered LCEs, azo-LCEs show an s-shaped stress-strain curve due to strain. At this time, the magnitude of the loading force is obtained immediately after the section in which the strain does not increase even with the increase in stress,

that is, the section in which the orientation changes is passed.

Among the samples of the three composition ratios used in this study, the azo-LCEs sample in which the ratio of EDDET and PETMP was 2 to 1 was polymerized showed a superior actuation rate compared to the other two samples. The cause can be identified through the real-time in situ test, and the key point lies in the nematic-isotropic phase transition caused by the transition temperature shifting. In the case of the sample, it was verified through the DMA strain test that it was completely changed to the nematic phase through a loading force of 0.05N, and photo-isomerization was performed under an external force. In general, in the case of a nematic phase having unidirectional orientation, the length is significantly longer than that of an isotropic phase without orientation. Therefore, in addition to the length contraction effect due to photo-isomerization, which has been verified through previous studies, the phase transition effect is applied overlappingly, resulting in a significantly larger change rate than other samples.

Chapter 6. Conclusion

In this study, we have successfully construct azobenzene incorporated liquid crystalline elastomers (azo-LCEs) system by using thiol-click polymerization reaction. Afterwards, the effect of the magnitude of the external force applied during photo actuation and the crosslinking density of azo-LCEs on the photo actuation tendency was measured using DMA and light sources of specific wavelengths. And also the isomer-interconnected feature is achieved by first synthesizing molecular-weight controlled azo-prepolymers. By using this method, the effect of isomer interconnection on the (thermo-) mechanical properties and photo-actuation responses are investigated and compared with the traditional random co-polymers. The azo-LCEs polymerized by thiol-ene Michael addition reaction exhibits superior properties such as photo-strain actuation (up to 26%) and work capacity (up to 0.077KJ/Kg). In this photo actuation process, transition temperature shifting occurs, and as a result, the phase change at the test temperature was measured through an in-situ test. As a result, azo-LCEs not only have considerable mechanical properties and actuation rates for soft applications, but also have a work capacity that exceeds the reported work capacity of mammalian muscles (0.039KJ/Kg). So it is expected to have potential as an artificial muscle capable of remote control.

국문 요약

광반응 탄성체 소재의 분자 네트워크 내부에 가교되어 있는 아조벤젠은 특정 파장대의 빛이 조사 될 경우 광 이성질화를 일으킵니다. 이러한 광 이성질화는 아조벤젠 그 자체의 구조 및 물성변화뿐 아니라, 분자배열 전체에 변화를 야기하여 결과적으로 물성변화와 거동을 발생시킵니다. 광반응 탄성체 소재의 이러한 가역성, 원격제어 가능성 및 그 응답이 즉각적이라는 특성으로 인해 소프트로봇, 정밀 센서 및 액츄에이터와 같은 다양한 활용이 기대되고 있습니다. 그러나 광반응 탄성체의 광변형 거동 시 그 변형의 크기가 충분하지 않고 발생하는 일의 크기가 제한적이라는 특성으로 인해 실질적인 활용에는 어려움을 겪고 있습니다.

이러한 한계점들을 해결하기 위해 본 연구에서는 Michael addition thiol-click 가교반응을 사용하여 액정 단량체, 아조벤젠 단량체, thiol 작용기를 지닌 가교제로 이루어진 광반응 탄성체 소재를 합성하였습니다. 외력에 의해 일시적인 배향성을 만들고 열을 통해 지울 수 있으며, 빛에 의해서도 형상기억사이클을 발생시키는 해당 광반응 탄성체는 외력하에서 26% 이상의 광반응 대변형을 발생시키며, 포유류근육이상의 일률을 발생시킬 수 있음을 확인하였습니다.

이 후 가교제의 조성비를 제어하는 것과 촉매와 작용기를 설정해주는 방식을 이용한 순차적 중합과정을 이용한 가교과정 제어를 통해 가교율을 통제하였고, 가교율의 변화에 따른 물성의 변화를 연구하였습니다. 또한 광반응에 따른 물성변화를 실시간으로 관측할 수 있는 실험환경을 구축하여, 광반응 거동 및 물성변화의 메커니즘을 규명하였습니다.

본 연구에서 소개한 광반응 탄성체 소재는 인공근육을 비롯한 다양한 응용분야에서 사용될 수 있는 조건을 가지고 있음을 보여주었을 뿐만 아니라, 향후 액츄에이터 및 그 메커니즘 연구를 위한 다양한 분야에서 중요하게 활용될 것으로 기대됩니다.

핵심단어: 탄성체 소재, 광반응 탄성체, 인공근육, 액츄에이터

학번: 2018-30325

Bibliography

1. Hyunhyub Ko, Ali Javey, Smart Acuators and Adhesives for Reconfigurable Matter. *Acc. Chem. Res*. **2017**, *50, 4*, 691 -702.

2. Manuel Schaffner, Jakob A. Faber, Lucas Pianegonda, Patrick A. Rühs, Fergal Coulter & André R. Studart. 3D printing of robotic soft actuators with programmable bioinspired architectures. *Nature Comm*. **2018**, 878.

3. Geoffey M. Spinks, Deforming Materials with Light: Photoresponsive Materials Muscle In On the Action. *Angewandte Chemie*. **2012**, *51, 10*, 2285-2287.

4. Christian Ohm, Martin Brehmer, Rudolf Zentel, Liquid Crystalline Elastomers as Actuators and Sensors. *Adv Mat.* **2010**, *22, 31*, 3366-3387.

5. Leonid Ionov, Polymeric Actuators. *Langmuir*. **2015**, *31, 18*, 5015-5024.

6. Leonid Ionov, Hydrogel-based actuators: possibilities and limitations. *Mat today.* **2014**, *17, 10*, 494-503.

7. H Jiang, C Li, X Huang, Actuators based on liquid crystalline elastomer materials, *Nanoscale*, **2013**, *5*, 5255-5240.

8. Brian M. Gillette, Jacob A. Jensen, Beixian Tang, Genevieve J. Yang, Ardalan Bazargan-Lari, Ming Zhong & Samuel K. Sia, In situ collagen assembly for integrating microfabricated three-dimensional cell-seeded matrices. *Nature Mat*, **2008**, *7*, 636-640.

9. Xiaobo Zhang, Zhibin Yu, Chuan Wang, David Zarrouk, Jung-Woo Ted Seo, Jim C. Cheng, Austin D. Buchan, Kuniharu Takei, Yang Zhao, Joel W. Ager, Junjun Zhang, Mark Hettick, Mark C. Hersam, Albert P. Pisano, Ronald S. Fearing & Ali Javey, Photoactuators and motors based on carbon nanotubes with selective chirality distributions. *Nature Comm*, **2014**, 2983.

10. Laurens T. de Haan, Julien M. N. Verjans, Dirk J. Broer, Cees W. M. Bastiaansen, and Albertus P. H. J. Schenning, Humidity-Responsive Liquid Crystalline Polymer Actuators with an Asymmetry in the Molecular Trigger That Bend, Fold, and Curl. *J. Am. Chem. Soc*. **2014**, *136, 30*, 10585-10588.

11. Y Bar-Cohen, EAP applications, potential, and challenges, Chapter, **2001**.

12. *Cutting Edge Chemistry*. The Royal Society of Chemistry: 2006.

13. Reinitzer, F., Beiträge zur Kenntniss des Cholesterins. *Monatshefte für Chemie und verwandte Teile anderer Wissenschaften* **1888,** *9* (1), 421-441.

14. Odian, G., Principles of Polymerization, Fourth Edition. **2004**, 1-38.

15. Hikmet, R. A. M.; Broer, D. J., Dynamic mechanical properties of anisotropic networks formed by liquid crystalline acrylates. *Polymer* **1991,** *32* (9), 1627-1632.

16. Varadan, V. K.; Varadan, V. V. Microsensors, microelectromechanical systems (MEMS), and electronics for smart structures and systems. *Smart Materials and Structures* **2000,** 9 (6), 953-972.

17. Palagi, S.; Mark, A. G.; Reigh, S. Y.; Melde, K.; Qiu, T.; Zeng, H.; Parmeggiani, C.; Martella, D.; Sanchez-Castillo, A.; Kapernaum, N.; Giesselmann, F.; Wiersma, D. S.; Lauga, E.; Fischer, P. Structured light enables biomimetic swimming and versatile locomotion of photoresponsive soft microrobots. *Nature Materials* **2016,** 15 (6), 647-+.

18. Ter Schiphorst, J.; Saez, J.; Diamond, D.; Benito-Lopez, F.; Schenning, A. Light-responsive polymers for microfluidic applications. *Lab Chip* **2018,** 18 (5), 699-709 DOI: 10.1039/c7lc01297g.

19. Lv, J.-a.; Liu, Y.; Wei, J.; Chen, E.; Qin, L.; Yu, Y. Photocontrol of fluid slugs in liquid crystal polymer microactuators. *Nature* **2016,** 537 (7619), nature19344 DOI: 10.1038/nature19344.

20. Gelebart, A. H.; Mulder, D. J.; Varga, M.; Konya, A.; Vantomme, G.; Meijer, E. W.; Selinger, R. L. B.; Broer, D. J. Making waves in a photoactive polymer film. *Nature* **2017,** 546 (7660), 632-+.

21. Liu, Y.; Shaw, B.; Dickey, M. D.; Genzer, J. Sequential self-folding of polymer sheets. *Science Advances* **2017,** 3 (3).

22. Bisoyi, H. K.; Urbas, A. M.; Li, Q. Soft Materials Driven by Photothermal Effect and Their Applications. *Advanced Optical Materials* **2018,** 6 (15), 1800458.

23. Tian, Q.; Fei, C.; Yin, H.; Feng, Y. Stimuli-responsive polymer wormlike micelles. *Progress in Polymer Science* **2019,** 89, 108-132.

24. Zeng, H.; Wani, O. M.; Wasylczyk, P.; Kaczmarek, R.; Priimagi, A. Self-Regulating Iris Based on Light-Actuated Liquid Crystal Elastomer. *Advanced Materials* **2017,** 29 (30), 1701814.

25. Weis, P.; Wu, S. Light-Switchable Azobenzene-Containing Macromolecules: From UV to Near Infrared. *Macromolecular Rapid Communications* **2018,** 39 (1), 1700220.

26. White, T. J.; Broer, D. J. Programmable and adaptive mechanics with liquid crystal polymer networks and elastomers. *Nature Materials* **2015,** 14 (11), 1087-1098-1098.

27. Hugel, T.; Holland, N. B.; Cattani, A.; Moroder, L.; Seitz, M.; Gaub, H. E. Single-Molecule Optomechanical Cycle. *Science* **2002,** 296 (5570), 1103-1106-1106.

28. Bisoyi, H.; Li, Q. Light-Driven Liquid Crystalline Materials: From Photo-Induced Phase Transitions and Property Modulations to Applications. *Chemical reviews* **2016,** 116 (24), 15089-15166-15166.

29. Ciferri, A. Translation of Molecular Order to the Macroscopic Level. *Chemical reviews* **2015**.

30. Naumov, P.; Chizhik, S.; Panda, M. K.; Nath, N. K.; Boldyreva, E. Mechanically Responsive Molecular Crystals. *Chemical Reviews* **2015,** 115 (22),

31. Han, D. D.; Zhang, Y. L.; Ma, J. N.; Liu, Y. Q.; Han, B.; Sun, H. B. Light-Mediated Manufacture and Manipulation of Actuators. *Advanced Materials* **2016,** 28 (38), 8328-8343-8343.

32. Bandara, H. M. D.; Burdette, S. C. Photoisomerization in different classes of azobenzene. *Chem. Soc. Rev.* **2012,** 41 (5), 1809-1825.

33. Crecca, C. R.; Roitberg, A. E. Theoretical study of the isomerization mechanism of azobenzene and disubstituted azobenzene derivatives. *J Phys Chem A* **2006,** 110 (26), 8188-8203.

34. Li, C.; Yun, J.-H.; Kim, H.; Cho, M., Light Propagation and Photoactuation in Densely Cross-Linked Azobenzene-Functionalized Liquid-Crystalline Polymers: Contribution of Host and Concerted Isomerism. *Macromolecules* **2016,** *49* (16), 6012-6020.

35. White, T. J.; Tabiryan, N. V.; Serak, S. V.; Hrozhyk, U. A.; Tondiglia, V. P.; Koerner, H.; Vaia, R. A.; Bunning, T. J., A high frequency photodriven polymer oscillator. *Soft Matter* **2008,** *4* (9), 1796-1798.

36. Lee, K. M.; Smith, M. L.; Koerner, H.; Tabiryan, N.; Vaia, R. A.; Bunning, T. J.; White, T. J., Photodriven, Flexural–Torsional Oscillation of Glassy Azobenzene Liquid Crystal Polymer Networks. *Advanced Functional Materials* **2011,** *21* (15), 2913-2918.

37. Iamsaard, S.; Aßhoff, S. J.; Matt, B.; Kudernac, T.; Cornelissen, J. J. L. M.; Fletcher, S. P.; Katsonis, N., Conversion of light into macroscopic helical motion. *Nature Chemistry* **2014,** *6* (3).

38. van Oosten, C. L.; Harris, K. D.; Bastiaansen, C. W. M.; Broer, D. J., Glassy photomechanical liquid-crystal network actuators for microscale devices. *The European physical journal. E, Soft matter* **2007,** *23* (3), 329-336.

39. Lee, K.; Smith, M. L.; Koerner, H.; Tabiryan, N.; Vaia, R. A.; Bunning, T. J.; White, T. J., Photodriven, Flexural–Torsional Oscillation of Glassy Azobenzene Liquid Crystal Polymer Networks. *Advanced Functional Materials* **2011,** *21* (15), 2913-2918.

40. Harris, K. D.; Cuypers, R.; Scheibe, P.; van Oosten, C. L.; Bastiaansen, C. W. M.; Lub, J.; Broer, D. J., Large amplitude light-induced motion in high elastic modulus polymer actuators. *Journal of Materials Chemistry* **2005,** *15* (47), 5043-5048.

41. Shen, WB, Du, B, Zhuo, HT, Chen, SJ, Recyclable and reprocessable epoxy-polyhedral oligomeric silsesquioxane (POSS)/mesogenic azobenzene/poly (ethylene-co-vinyl acetate) composites with thermal- and light-responsive programmable shape-memory performance. *Chem Eng Journal*, **2022,** *132609, 428.*

42. Ristola, M, Fedele, C, Hagman,S, Narkilahti, S. Directional Growth of Human Neuronal Axons in a Microfluidic Device with Nanotopography on Azobenzene-Based Material. *Adv Mat Interfaces*, **2021**, 8, 11.

43. Finkelmann, H.; Nishikawa, E.; Pereira, G. G.; Warner, M., A new opto-mechanical effect in solids. **2001**.

44. Yu, Y.; Nakano, M.; Ikeda, T., Photomechanics: Directed bending of a polymer film by light. *Nature* **2003,** *425* (6954).

45. J Yun. Presentation document, *Seoul National University*, **2019.**

46. Cho, Eun-hye, Khuong Luu, and Soo-young Park. Mechano-actuated light-responsive main-chain liquid crystal elastomers. *Macromolecules*, **2021**, 5397-5409.

47. Li, C.; Yun, J. H.; Kim, H.; Cho, M. Light Propagation and Photoactuation in Densely Cross-Linked Azobenzene-Functionalized Liquid-Crystalline Polymers: Contribution of Host and Concerted Isomerism. *Macromolecules* **2016,** 49 (16), 6012-6020.

48. Li, C., Moon, J., Yun, J. H., Kim, H., & Cho, M. Influence of external loads on structure and photoactuation in densely crosslinked azo-incorporated liquid crystalline polymers. *Polymer*, **2017**, 129, 252-260.

49. Koulouri, E. G.; Kallitsis, J. K.; Hadziioannou, G. Terminal anhydride functionalized polystyrene by atom transfer radical polymerization used for the compatibilization of nylon 6/PS blends. *Macromolecules* **1999,** 32 (19), 6242-6248.

50. Matyjaszewski, K. Atom Transfer Radical Polymerization (ATRP): Current Status and Future Perspectives. *Macromolecules* **2012,** 45 (10), 4015-4039.

51. Niu, X.; Yang, X.; Brochu, P.; Stoyanov, H.; Yun, S.; Yu, Z.; Pei, Q. Bistable Large-Strain Actuation of Interpenetrating Polymer Networks. *Advanced Materials* **2012,** 24 (48), 6513-6519.

52. Ube, T.; Minagawa, K.; Ikeda, T. Interpenetrating polymer networks of liquid-crystalline azobenzene polymers and poly(dimethylsiloxane) as photomobile materials. *Soft Matter* **2017,** 13 (35), 5820-5823.

53. Lu, H.-F.; Wang, M.; Chen, X.-M.; Lin, B.-P.; Yang, H. Interpenetrating Liquid-Crystal Polyurethane/Polyacrylate Elastomer with Ultrastrong Mechanical Property. *Journal of the American Chemical Society* **2019.**

54. Badi, N.; Lutz, J. F. Sequence control in polymer synthesis. *Chem Soc Rev* **2009,** 38 (12), 3383-3390.

55. Lutz, J. F.; Ouchi, M.; Liu, D. R.; Sawamoto, M. Sequence-Controlled Polymers. *Science* **2013,** 341 (6146), 628-+.

56. Yu, B.; Chan, J. W.; Hoyle, C. E.; Lowe, A. B. Sequential thiol-ene/thiol-ene and thiol-ene/thiol-yne reactions as a route to well-defined mono and bis end-functionalized poly(N-isopropylacrylamide). *Journal of Polymer Science Part A: Polymer Chemistry* **2009,** 47 (14), 3544-3557.

57. Lowe, A. B. Thiol-ene "click" reactions and recent applications in polymer and materials synthesis. *Polymer Chemistry* **2010,** 1 (1), 17-36.

58. Lowe, A. B. Thiol-ene "click" reactions and recent applications in polymer and materials synthesis: a first update. *Polymer Chemistry* **2014,** 5 (17), 4820-4870.

59. Peng, H.; Nair, D. P.; Kowalski, B. A.; Xi, W.; Gong, T.; Wang, C.; Cole, M.; Cramer, N. B.; Xie, X.; McLeod, R. R.; Bowman, C. N. High Performance Graded Rainbow Holograms via Two-Stage Sequential Orthogonal Thiol–Click Chemistry. *Macromolecules* **2014,** 47 (7), 2306-2315.

60. Nair, D. P.; Podgorski, M.; Chatani, S.; Gong, T.; Xi, W. X.; Fenoli, C. R.; Bowman, C. N. The Thiol-Michael Addition Click Reaction: A Powerful and Widely Used Tool in Materials Chemistry. *Chemistry of Materials* **2014,** 26 (1), 724-744.

61. Cramer, N. B.; Bowman, C. N. Kinetics of thiol-ene and thiol-acrylate photopolymerizations with real-time fourier transform infrared. *Journal of Polymer Science Part A: Polymer Chemistry* **2001,** 39 (19), 3311-3319.